

# A New 5 Flavour NLO Analysis and Parametrizations of Parton Distributions of the Real Photon

F.Cornet<sup>a</sup>, P.Jankowski<sup>b</sup> and M.Krawczyk<sup>b</sup>

<sup>a</sup>*Departamento de Física Teórica y del Cosmos, Universidad de Granada,  
Campus de Fuente Nueva, E-18071, Granada, Spain*

<sup>b</sup>*Institute of Theoretical Physics, Warsaw University,  
ul. Hoża 69, 00-681 Warsaw, Poland*

## Abstract

New, radiatively generated, NLO quark ( $u, d, s, c, b$ ) and gluon densities in a real, unpolarized photon are presented. We perform three global fits, based on the NLO DGLAP evolution equations for  $Q^2 > 1$  GeV<sup>2</sup>, to all the available structure function  $F_2^\gamma(x, Q^2)$  data. As in our previous LO analysis we utilize two theoretical approaches. Two models, denoted as FFNS<sub>CKJ1</sub> & 2 NLO, adopt the so-called Fixed Flavour-Number Scheme for calculation of the heavy-quark contributions to  $F_2^\gamma(x, Q^2)$ , the CJK NLO model applies the ACOT( $\chi$ ) scheme. We examine the results of our fits by a comparison with the LEP data for the  $Q^2$  dependence of the  $F_2^\gamma$ , averaged over various  $x$ -regions, and the  $F_{2,c}^\gamma$ . Grid parametrizations of the parton densities for all fits are provided.

# 1 Introduction

In this work we extend the LO QCD analysis of the structure function  $F_2^\gamma(x, Q^2)$  of the unpolarized real photon [1–3], to the Next-to-Leading order (NLO). As before we are especially interested in the description of the charm- and beauty-quark contributions to  $F_2^\gamma(x, Q^2)$ . We adopt two approaches, the FFNS<sub>CJK</sub> and CJK ones, as discussed in [1] and (with some modifications) in [2]. In the first model, referred to as FFNS<sub>CJK1</sub> NLO, we adopt a standard approach in which a heavy quark,  $h$ , contributes to the photon structure function only through the 'direct' (Bethe-Heitler)  $\gamma^* + \gamma \rightarrow h + \bar{h}$  process and the process with 'resolved photon'  $\gamma^* + G^\gamma \rightarrow h + \bar{h}$ . In the FFNS<sub>CJK2</sub> NLO model we include in addition  $\gamma^* + G^\gamma \rightarrow h + \bar{h} + G$  and  $\gamma^* + q^\gamma(\bar{q}^\gamma) \rightarrow q(\bar{q}) + h + \bar{h}$  processes<sup>1</sup>. In the third model, CJK NLO, we use the ACOT( $\chi$ ) scheme [4] in which, apart from the direct and resolved photon  $O(\alpha_s)$  contributions<sup>2</sup>, we deal with the heavy-quark densities  $q_h(x, Q^2)$ . The subtraction of the double counted terms as well as introduction of a new kinematic variable  $\chi_h$  improve description of  $F_2^\gamma(x, Q^2)$  in both regions: below and above the heavy-quark thresholds.

In [1–3] we followed the idea of the radiatively generated parton distributions introduced by the GRV group first to describe nucleon [5] and pion [6] and later used for the real [7], [8] and virtual photon [8], [9]. In our LO analyses [1–3] we used  $Q_0^2 = 0.25$  GeV<sup>2</sup> and adopted the input distributions of the valence-type form introduced in [7] neglecting sea-quark densities. In the case of the NLO analysis we found that the starting scale of the evolution appears to tend to higher values,  $Q_0^2 \approx 0.7$  GeV<sup>2</sup> (similarly as in [10]). We tested the assumption on vanishing sea-quark densities at  $Q_0^2$  by performing additional fits.

All our global fits are performed at  $Q^2 > 1$  GeV<sup>2</sup> utilizing the set of all available  $F_2^\gamma(x, Q^2)$  data.

We test our results for  $F_2^\gamma(x, Q^2)$  by comparing them with the LEP data which were not used in the fits: for the  $Q^2$  dependence of the  $F_2^\gamma$ , averaged over various  $x$ -regions, and for the  $F_{2,c}^\gamma$  data.

Our paper is divided into six parts. In section 2 we shortly recall basic schemes applied to calculation of the heavy-quark production in the Deep Inelastic Scattering on the real-photon target. Section 3 is devoted to the description of the FFNS<sub>CJK</sub> NLO models of the  $F_2^\gamma(x, Q^2)$ . Next, the CJK NLO model based on the ACOT( $\chi$ ) scheme [4] is presented in detail. In section 4 we describe the solutions of the DGLAP evolution equations in all models and assumptions for the input parton densities. Results of the global fits are discussed and compared with the  $F_2^\gamma(x, Q^2)$ ,  $F_2^\gamma(Q^2)$  and  $F_{2,c}^\gamma$  data in the fifth section of the paper. We end our paper by presenting in the Appendix the technical details of the calculation. The parton distributions resulting from our fits have been parametrized on the grid.

---

<sup>1</sup>These two FFNS<sub>CJK1</sub> & 2 models differ from the corresponding models introduced in our LO analysis.

<sup>2</sup>Inclusion of the  $O(\alpha_s^2)$  terms in the CJK NLO approach is beyond the scope of this work.

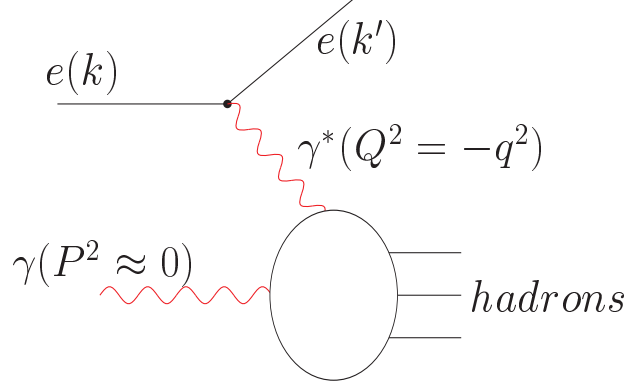


Figure 1: Deep Inelastic Scattering on quasi real photon ( $P^2 \approx 0$ ),  $e + \gamma \rightarrow e + \text{hadrons}$ .

## 2 Production of heavy quarks in $\text{DIS}_{e\gamma}$

The Deep Inelastic Scattering on a photon ( $\text{DIS}_{e\gamma}$ ) allows to measure the structure function  $F_2^\gamma$ , and others, via the process

$$e + \gamma \rightarrow e + \text{hadrons}, \quad (1)$$

presented in the figure 1. The differential cross-section for this process is given by:

$$\frac{d\sigma^{e\gamma \rightarrow eX}}{dxdy} = \frac{2\pi\alpha^2}{xyQ^2} [(1 + (1 - y)^2)F_2^\gamma(x, Q^2) - y^2F_L^\gamma(x, Q^2)], \quad (2)$$

where  $x$  and  $y$  are the standard  $\text{DIS}_{e\gamma}$  variables, defined through the virtuality  $Q^2$  of the probing photon and momenta of interacting particles shown in figure 1,

$$x = \frac{Q^2}{2p \cdot q}, \quad y = \frac{p \cdot q}{p \cdot k}, \quad (3)$$

and  $F_L^\gamma(x, Q^2)$  is the so-called longitudinal structure function corresponding to the exchange of the longitudinally polarized  $\gamma^*$ . For the presently kinematically accessible values of  $y$  the  $F_L^\gamma(x, Q^2)$  contribution is negligible.

Each of partons (quarks and gluon) of the real photon contributes to the  $F_2^\gamma(x, Q^2)$  proportionally to the corresponding partonic cross-section. The calculation of the light  $u$ -,  $d$ -,  $s$ -quark and gluon cross-sections is straightforward.

Various schemes used in the calculation of the heavy-quark production have been described in [1]. They are also explained in the vast literature, [4], [11] and [12]. Let us shortly recall the main facts on the FFNS and ACOT( $\chi$ ) approaches applied in this analysis.

There exist two standard schemes in a calculation of a heavy-quark,  $h$ , production at the hard scale  $\mu$ . In both of them the light quarks  $u$ ,  $d$  and  $s$  are treated as massless because for them  $\mu \gg \Lambda_{QCD} > m_q$ , where  $m_q$  is a light-quark mass. In the case of the DIS process the hard scale  $\mu$  is identified with the virtuality of the probing photon,

$\mu^2 = Q^2$ . In the massive Fixed Flavour-Number Scheme (FFNS) heavy  $c$ - and  $b$ -quarks are treated differently: the massive charm and beauty quarks produced in hard subprocesses  $\gamma^* + \gamma \rightarrow h + \bar{h}$  can only appear in the final state. In the second, massless scheme, called the Zero-mass Variable Flavour-Number Scheme (ZVFNS) heavy-quark distributions appear alike the light-parton densities. When  $Q^2$  is larger than a threshold associated with a heavy quark (usually taken as  $Q^2 = m_h^2$ ), this quark is considered as an extra massless parton in addition to the three light quarks. This way, the number of different types of quarks (flavours) increases with increasing  $Q^2$ . One introduces a notion of “active quarks”, for which the condition  $Q^2 > m_q^2$  is fulfilled and which can be treated as massless partons of the probed real photon. When active, their densities  $q_i(x, Q^2)$  differ from zero, otherwise  $q_i(x, Q^2) = 0$ .

The above standard schemes are considered to be reliable in different  $Q^2$  regions. The FFNS loses its descriptive power when  $Q^2 \gg m_h^2$ , on the other hand the ZVFNS does not seem appropriate if  $Q^2 \approx m_h^2$ . To obtain a prescription working for all hard scales one needs to combine features of both schemes. There exist the whole set of the approaches, generally denoted as General-mass Variable Flavour-Number Schemes (GVFNS), which in the  $Q^2 \rightarrow m_h^2$  and  $Q^2 \rightarrow \infty$  limits reproduce the behaviour of the FFNS and ZVFNS schemes respectively. Their recent realization is the so-called ACOT( $\chi$ ) scheme introduced for the proton structure function in [4] and used by us in our LO analysis [1–3].

In the ACOT( $\chi$ ) scheme, all contributions to the considered process, which would be included separately in the ZVFNS and FFNS, are taken into account. Such procedure requires proper subtraction of double counted contributions, i.e. the large logarithms which appear in the massive heavy-quark Wilson coefficients (the FFNS scheme) but are also resummed in the  $q_h(x, \mu^2)$  densities. That way one obtains a scheme in principle appropriate in the whole  $Q^2$  range. Still, another problem emerges. In any process the kinematical threshold for the heavy-quark production is given by the total energy of that process,  $W$ . Obviously  $W$  must be greater than two masses of the heavy quark in hand,  $W > 2m_h$ , so in the  $\text{DIS}_{e\gamma}$  case where the hard scale is  $Q^2$ , we have  $W^2 = (1-x)Q^2/x > 4m_h^2$ . As  $\mu^2 = Q^2$  the ZVFNS condition  $\mu > m_h$  (or any similar) for treating a heavy quark  $h$  as a massless parton is not correct. It may happen (for small enough  $x$ ) that  $q_h(x, Q^2) = 0$  in the kinematically allowed region  $W > 2m_h$ . On the other hand, we can also obtain nonzero heavy-quark densities in the kinematically forbidden  $(x, Q^2)$  region. The ACOT( $\chi$ ) scheme solves this problems through introduction of a new variable  $\chi_h \equiv x(1 + 4m_h^2/Q^2)$  which replaces in the ZVFNS the Bjorken  $x$  as an argument of the heavy-parton density.

In the next sections we will present the realizations of the FFNS and ACOT( $\chi$ ) schemes for the calculation of the photon structure  $F_2^\gamma$  in the Next-to-Leading order of QCD, namely our  $\text{FFNS}_{CJK}$  NLO and CJK NLO models.

### 3 Description of the $F_2^\gamma$ in the $\text{FFNS}_{CJK}$ NLO

This section is devoted to the  $\text{FFNS}_{CJK}1 \& 2$  NLO models, which are the realizations of the FFNS approach for the photon structure  $F_2^\gamma$  in the Next-to-Leading Order of QCD.

The only difference between this two models is following: the  $\text{FFNS}_{CJK}\text{NLO 2}$  approach includes additional higher order contributions to  $F_2^\gamma$  neglected in the  $\text{FFNS}_{CJK}\text{NLO 1}$  model.

First, we describe the light-quark contributions to  $F_2^\gamma(x, Q^2)$  which are common for the both analysed models. Next, we discuss the heavy-quark contributions for the  $\text{FFNS}_{CJK}\text{NLO}$  approach. Further, we recall the  $\text{DIS}_\gamma$  factorization scheme used in the model and resume by giving the final formulae for the  $F_2^\gamma(x, Q^2)$  in the  $\text{FFNS}_{CJK}$  NLO models.

### 3.1 Light-quark contributions

In the Next-to-Leading Order logarithmic approximation of QCD or, in short, in NLO QCD the light-quark contributions to the photon structure function  $F_2^\gamma(x, Q^2)$  can be written in terms of light-quark ( $u, d$  and  $s$ ) densities  $q_i^\gamma(x, Q^2)$  as follows:

$$\begin{aligned} \frac{1}{x} F_2^\gamma(x, Q^2) |_{light} &= \sum_{i=1}^3 e_i^2 \left\{ (q_i^\gamma + \bar{q}_i^\gamma)(x, Q^2) + e_i^2 \frac{\alpha}{2\pi} C_{2,\gamma}^{(0)}(x) \right. \\ &+ \left. \frac{\alpha_s(Q^2)}{2\pi} \int_x^1 \frac{dy}{y} \left[ (q_i^\gamma + \bar{q}_i^\gamma)(y, Q^2) C_{2,q}^{(1)}\left(\frac{x}{y}\right) + G^\gamma(y, Q^2) C_{2,G}^{(1)}\left(\frac{x}{y}\right) \right] \right\}. \end{aligned} \quad (4)$$

Note, that  $q_i^\gamma(x, Q^2) = \bar{q}_i^\gamma(x, Q^2)$ . The  $C_{2,j}^{(i)}(x)$  functions are the  $O(\alpha_s^i)$  order terms of the hadronic (Wilson) coefficient functions ( $j = \gamma, q, G$ )

$$C_{2,j}(x, Q^2) = C_{2,j}^{(0)}(x) + \frac{\alpha_s(Q^2)}{2\pi} C_{2,j}^{(1)}(x) + \dots \quad (5)$$

Each of them is related to the hard process of a parton originating from the real photon (for instance quark for  $C_{2,q}(x)$ ) interacting with the virtual photon. The coefficients appearing in Eq. (4) are listed in table 1. The formulae for the  $C_{2,j}^{(i)}(x)$  functions up to the  $O(\alpha_s^2)$  order can be found in [13], see also the Appendix.

order	hard (parton) process	coefficient function
$O(\alpha_s^0)$	$\gamma^* + q^\gamma(\bar{q}^\gamma) \rightarrow q(\bar{q})$	$C_{2,q}^{(0)}(x) = \delta(1-x)$
	$\gamma^* + \gamma \rightarrow q + \bar{q}$	$C_{2,\gamma}^{(0)}(x)$
$O(\alpha_s^1)$	$\gamma^* + q^\gamma(\bar{q}^\gamma) \rightarrow q(\bar{q}) + G$	$C_{2,q}^{(1)}(x)$
	$\gamma^* + G^\gamma \rightarrow q + \bar{q}$	$C_{2,G}^{(1)}(x)$

Table 1: Hard parton processes and the corresponding Wilson coefficient functions for light quarks.

The evolution of the parton densities in  $\ln Q^2$  is governed by the inhomogeneous

DGLAP equations [14]. In the NLO we have:

$$\begin{aligned}
\frac{dq_i^\gamma(x, Q^2)}{d \ln Q^2} &= \frac{\alpha}{2\pi} e_i^2 k_q(x, Q^2) \\
&+ \frac{\alpha_s(Q^2)}{2\pi} \int_x^1 \frac{dy}{y} \left\{ \sum_{k=1}^{N_f} \left[ q_k^\gamma(y, Q^2) P_{q\bar{q}}\left(\frac{x}{y}, Q^2\right) + \bar{q}_k^\gamma(y, Q^2) P_{q\bar{q}}\left(\frac{x}{y}, Q^2\right) \right] + G^\gamma(y, Q^2) P_{qG}\left(\frac{x}{y}, Q^2\right) \right\}, \\
\frac{dG^\gamma(x, Q^2)}{d \ln Q^2} &= \frac{\alpha}{2\pi} k_G(x, Q^2) \\
&+ \frac{\alpha_s(Q^2)}{2\pi} \int_x^1 \frac{dy}{y} \left\{ \sum_{k=1}^{N_f} \left[ q_k^\gamma(y, Q^2) P_{Gq}\left(\frac{x}{y}, Q^2\right) + \bar{q}_k^\gamma(y, Q^2) P_{G\bar{q}}\left(\frac{x}{y}, Q^2\right) \right] + G^\gamma(y, Q^2) P_{GG}\left(\frac{x}{y}, Q^2\right) \right\}
\end{aligned}
\quad (6) \quad (7)$$

where  $N_f$  is a number of active quarks. Here  $N_f = 3$  as all heavy-quark densities are equal zero in the FFNS models. The functions  $P_{ij}(x, Q^2)$  and  $k_i(x, Q^2)$  are the NLO splitting functions

$$\begin{aligned}
k_i(x, Q^2) &= k_i^{(0)}(x) + \frac{\alpha_s(Q^2)}{2\pi} k_i^{(1)}(x), \\
P_{ij}(x, Q^2) &= P_{ij}^{(0)}(x) + \frac{\alpha_s(Q^2)}{2\pi} P_{ij}^{(1)}(x).
\end{aligned}
\quad (8)$$

The  $k_q(x, Q^2)$  and  $k_G(x, Q^2)$  are referred to as the photon-quark and photon-gluon splitting functions, respectively. Up to the NLO order  $P_{Gq} = P_{G\bar{q}}$ . Formulae for  $O(\alpha_s)$  and  $O(\alpha_s^2)$  splitting functions can be found for instance in [15].

### 3.2 Heavy-quark contributions

In the FFNS models heavy quarks appear only in the final state of the process and the density functions  $q_h(x, Q^2)$  are equal to zero. The charm- and beauty-quark contributions to the structure function are described by the heavy-quark coefficient functions  $C_{2,j}^{h,(i)}$  related to the hard processes as listed in table 2. One obtains

$$\begin{aligned}
\frac{1}{x} F_2^\gamma(x, Q^2)|_{heavy, FFNS} &= \sum_{h=c,b}^2 e_h^2 \left\{ \frac{\alpha_s(Q^2)}{2\pi} \int_{\chi_h}^1 \frac{dy}{y} G^\gamma(y, Q^2) C_{2,G}^{h,(1)}\left(\frac{x}{y}, \frac{Q^2}{m_h^2}\right) + e_h^2 \frac{\alpha}{2\pi} C_{2,\gamma}^{h,(0)}(x, \frac{Q^2}{m_h^2}) \right\} \\
&+ \sum_{h=c,b}^2 \left\{ \left( \frac{\alpha_s(Q^2)}{2\pi} \right)^2 \int_{\chi_h}^1 \frac{dy}{y} \left[ \sum_{i=1}^3 (q_i^\gamma + \bar{q}_i^\gamma)(y, Q^2) (e_i^2 C_{2,q}^{(2)}\left(\frac{x}{y}, \frac{Q^2}{m_h^2}\right) + e_h^2 C_{2,q}^{h,(2)}\left(\frac{x}{y}, \frac{Q^2}{m_h^2}\right)) \right. \right. \\
&\quad \left. \left. + e_h^2 G^\gamma(y, Q^2) C_{2,G}^{h,(2)}\left(\frac{x}{y}, \frac{Q^2}{m_h^2}\right) \right] + \frac{\alpha \alpha_s(Q^2)}{(2\pi)^2} e_h^4 C_{2,\gamma}^{h,(1)}(x, \frac{Q^2}{m_h^2}) \right\},
\end{aligned}
\quad (9)$$

where the parameter  $\chi_h = x(1 + 4m_h^2/Q^2)$  takes care of the proper region of the integration.

We consider two FFNS models, FFNS<sub>CJK1</sub> and FFNS<sub>CJK2</sub> NLO, where only in the latter we include the  $O(\alpha_s^2)$  and  $O(\alpha \alpha_s)$  contributions to  $F_2^\gamma$ . The reason for

order	parton subprocess	coefficient function
$O(\alpha_s^0)$	$\gamma^* + \gamma \rightarrow h + \bar{h}$	$C_{2,\gamma}^{h,(0)}$
$O(\alpha_s^1)$	$\gamma^* + G^\gamma \rightarrow h + \bar{h}$	$C_{2,G}^{h,(1)}$
	$\gamma^* + \gamma \rightarrow h + \bar{h} + G$	$C_{2,\gamma}^{h,(1)}$
$O(\alpha_s^2)$	$\gamma^* + G^\gamma \rightarrow h + \bar{h} + G$	$C_{2,G}^{h,(2)}$
	$\gamma^* + q^\gamma(\bar{q}^\gamma) \rightarrow q(\bar{q}) + h + \bar{h}$	$C_{2,q}^{h,(2)}, C_{2,q}^{(2)}$

Table 2: Hard parton processes and the corresponding Wilson coefficient functions for heavy quarks.

considering two models is twofold. First, to check the size of the higher order heavy-quark contributions. Secondly, to perform a test whether the  $O(\alpha_s^2)$  and  $O(\alpha\alpha_s)$  terms should be included in the calculations as they are of higher order than the other NLO contributions.

Let us notice that among the higher order terms there appear two Wilson coefficients originating from the process  $\gamma^* + q^\gamma(\bar{q}^\gamma) \rightarrow q(\bar{q}) + h + \bar{h}$ , the  $C_{2,q}^{h,(2)}$  and  $C_{2,q}^{(2)}$  (see Fig. 2), the interference term of two diagrams (proportional to  $e_h e_q$ ) gives 0 according to [13].

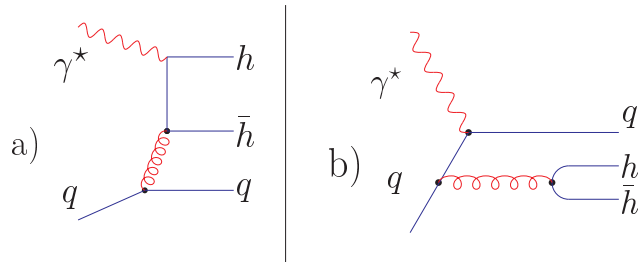


Figure 2: Diagrams relevant for  $\gamma^* + q^\gamma(\bar{q}^\gamma) \rightarrow q(\bar{q}) + h + \bar{h}$  process corresponding to a) the  $C_{2,q}^{h,(2)}$  coefficient and b) the  $C_{2,q}^{(2)}$  coefficient.

### 3.3 The $\overline{\text{MS}}$ and $\text{DIS}_\gamma$ factorization schemes

All the splitting and coefficient functions introduced in former sections have been derived in the modified minimal subtraction factorization scheme ( $\overline{\text{MS}}$ ). (They all can be found in the literature, see Appendix A). Let us notice that the  $C_{2,\gamma}^{(0)}(x)$  term in Eq. 4, describing the 'direct' contribution of the photon to  $F_2^\gamma(x, Q^2)$  causes a problem in the  $\overline{\text{MS}}$  scheme [16]. Firstly, contrary to all other contributions, this term does not vanish at the input scale  $Q_0^2$ . One obtains very different boundary conditions for the light-quark contribution in LO and NLO:

$$\frac{1}{x} F_2^\gamma(x, Q_0^2)|_{\text{light}} = \begin{cases} 0 & , \text{LO} \\ \sum_{i=1}^3 e_i^4 \frac{\alpha}{2\pi} C_{2,\gamma}^{(0)}(x) & , \text{NLO.} \end{cases} \quad (10)$$

This leads to very distinct results over the whole  $x$ -range (see for instance [17]). The heavy-quark contributions,  $C_{2,\gamma}^{h,(k)}(x, \frac{Q^2}{m_h^2})$ , for  $k = 0, 1$ , of Eq. (9) do not cause a similar problem as the  $O(\alpha_s^0)$  term appears already in the LO calculation and the  $C_{2,\gamma}^{h,(1)}(x, \frac{Q^2}{m_h^2})$  coefficient is only its  $O(\alpha_s^1)$  correction.

Secondly, the  $C_{2,\gamma}^{(0)}(x)$  term calculated in the  $\overline{\text{MS}}$  scheme is negative and divergent in the large- $x$  region, where  $C_{2,\gamma}^{(0)}(x) \simeq 3[\ln(1-x) - 1]$ , leading to unphysical negative values of  $F_2^\gamma$  at  $x \rightarrow 1$ . It is not cured by addition of other NLO contributions to the structure function as they all vanish at  $x = 1$  (if a typical choice of the shape of the hadronic input is made).

In a new factorization scheme, denoted as  $\text{DIS}_\gamma$ , introduced in [16], one avoids the troubles connected with the  $C_{2,\gamma}^{(0)}(x)$  term by absorbing it into the quark distributions  $q_i^\gamma(x, Q^2)$ , namely

$$\begin{aligned} q_i^{\text{DIS}_\gamma}(x, Q^2) &= q_i^{\overline{\text{MS}}}(x, Q^2) + e_i^2 \frac{\alpha}{4\pi} C_{2,\gamma}^{(0),\overline{\text{MS}}}(x), \\ C_{2,\gamma}^{(0),\text{DIS}_\gamma}(x) &= C_{2,\gamma}^{(0),\overline{\text{MS}}}(x) + \Delta C_{2,\gamma}^{(0)}(x) = 0, \end{aligned} \quad (11)$$

where obviously

$$\Delta C_{2,\gamma}^{(0)}(x) = C_{2,\gamma}^{(0),\overline{\text{MS}}}(x). \quad (12)$$

The gluon density and other coefficient functions are unaltered by the above redefinition but it leads to a modification of the photon-quark and photon-gluon splitting functions appearing in the DGLAP evolution of the parton distributions:

$$\begin{aligned} k_q^{(1),\text{DIS}_\gamma}(x, Q^2) &= k_q^{(1),\overline{\text{MS}}}(x, Q^2) - \frac{1}{2} \int_x^1 \frac{dy}{y} P_{qq}^{(0)}\left(\frac{x}{y}\right) C_{2,\gamma}^{(0),\text{DIS}_\gamma}(y), \\ k_G^{(1),\text{DIS}_\gamma}(x, Q^2) &= k_G^{(1),\overline{\text{MS}}}(x, Q^2) - \sum_{i=1}^{N_f} e_i^2 \int_x^1 \frac{dy}{y} P_{Gq}^{(0)}\left(\frac{x}{y}\right) C_{2,\gamma}^{(0),\text{DIS}_\gamma}(y). \end{aligned} \quad (13)$$

In our analysis we apply the  $\text{DIS}_\gamma$  factorization scheme, for simplicity the  $\text{DIS}_\gamma$  superscript will be omitted below, if possible.

### 3.4 Formulae for $F_2^\gamma$

$F_2^\gamma(x, Q^2)$  in the FFNS<sub>CKJNLO 1</sub> model reads;

$$\begin{aligned} & \frac{1}{x} F_2^\gamma(x, Q^2) |_{\text{FFNS}1} = \\ & \sum_{i=1}^3 e_i^2 \left\{ (q_i^\gamma + \bar{q}_i^\gamma)(x, Q^2) + \frac{\alpha_s(Q^2)}{2\pi} \int_x^1 \frac{dy}{y} \left[ (q_i^\gamma + \bar{q}_i^\gamma)(y, Q^2) C_{2,q}^{(1)}\left(\frac{x}{y}\right) + G^\gamma(y, Q^2) C_{2,G}^{(1)}\left(\frac{x}{y}\right) \right] \right\} \\ & + \sum_{h=c,b}^2 e_h^2 \left\{ \frac{\alpha_s(Q^2)}{2\pi} \int_{\chi_h}^1 \frac{dy}{y} G^\gamma(y, Q^2) C_{2,G}^{h,(1)}\left(\frac{x}{y}, \frac{Q^2}{m_h^2}\right) + e_h^2 \frac{\alpha}{2\pi} C_{2,\gamma}^{h,(0)}\left(x, \frac{Q^2}{m_h^2}\right) \right\}. \end{aligned} \quad (14)$$

In the case of the  $F_2^\gamma(x, Q^2)|_{FFNS2}$  model we include the  $O(\alpha_s^2)$  and  $O(\alpha\alpha_s)$  terms, obtaining

$$\begin{aligned} \frac{1}{x}F_2^\gamma(x, Q^2)|_{FFNS2} &= \frac{1}{x}F_2^\gamma(x, Q^2)|_{FFNS1} \\ &+ \sum_{h=c,b}^2 \left\{ \left( \frac{\alpha_s(Q^2)}{2\pi} \right)^2 \int_{\chi_h}^1 \frac{dy}{y} \left[ \sum_{i=1}^3 (q_i^\gamma + \bar{q}_i^\gamma)(y, Q^2) (e_i^2 C_{2,q}^{(2)}(\frac{x}{y}, \frac{Q^2}{m_h^2}) + e_h^2 C_{2,q}^{h,(2)}(\frac{x}{y}, \frac{Q^2}{m_h^2})) \right. \right. \\ &\quad \left. \left. + e_h^2 G^\gamma(y, Q^2) C_{2,G}^{h,(2)}(\frac{x}{y}, \frac{Q^2}{m_h^2}) \right] + \frac{\alpha\alpha_s(Q^2)}{(2\pi)^2} e_h^4 C_{2,\gamma}^{h,(1)}(x, \frac{Q^2}{m_h^2}) \right\}. \end{aligned} \quad (15)$$

## 4 Description of the $F_2^\gamma$ in the CJK NLO model

This section is devoted to the description of the CJK NLO model based on the ACOT( $\chi$ ) approach. The approach combines the FFNS scheme introduced in the former section with the ZVFNS scheme in which heavy quarks are treated in the similar way as the light ones.

### 4.1 Light-quark contributions

The light-quark contributions to  $F_2^\gamma$  are the same in FFNS and ZVFNS schemes and were already given in Eq. (4) for the  $\overline{\text{MS}}$  factorization scheme and in Eq. (14) for the  $\text{DIS}_\gamma$  scheme. The difference between the numerical values of those contributions originates from the difference between the number of the active quarks,  $N_f$ , in the DGLAP equations in both approaches. We have  $N_f = 3$  for the  $\text{FFNS}_{CJK}$  NLO models, while  $N_f = 5$  in the CJK NLO model.

### 4.2 Heavy-quark contributions

Apart from the heavy-quark terms which properly describe the  $h$ -quark contributions to  $F_2^\gamma(x, Q^2)$ , in the corresponding  $Q^2 \approx m_h^2$  regions, are given by the FFNS formula (9). Let us only notice that in the CJK NLO model case we neglect the  $O(\alpha_s^2)$  and  $O(\alpha\alpha_s)$  contributions to  $F_2^\gamma(x, Q^2)|_{heavy,FFNS}$ . They lead to a very complicated expression for  $F_2^\gamma(x, Q^2)$  and their analysis is beyond the scope of this work. As already discussed, the FFNS scheme loses its descriptive power if  $Q^2 \gg m_h^2$ . Therefore, the addition of the ZVFNS terms, the massless charm- and beauty-quark distributions,  $q_h(x, Q^2)$ , in the photon, appropriate in that region, is needed. They are combined with the light-quark densities through the DGLAP equations with  $N_f = 5$  active quarks. In the ZVFNS approach heavy-quark contributions to  $F_2^\gamma(x, Q^2)$  read

$$\begin{aligned} \frac{1}{x}F_2^\gamma(x, Q^2)|_{heavy,ZVFNS} &= \sum_{h=c,b}^2 e_h^2 \left\{ (q_h^\gamma + \bar{q}_h^\gamma)(x, Q^2) + e_h^2 \frac{\alpha}{2\pi} C_{2,\gamma}^{(0)}(x) \right. \\ &\quad \left. + \frac{\alpha_s(Q^2)}{2\pi} \int_x^1 \frac{dy}{y} \left[ (q_h^\gamma + \bar{q}_h^\gamma)(y, Q^2) C_{2,q}^{(1)}(\frac{x}{y}) + G^\gamma(y, Q^2) C_{2,G}^{(1)}(\frac{x}{y}) \right] \right\}. \end{aligned} \quad (16)$$

### 4.3 Subtraction terms

A simple summing of all the discussed terms, namely

$$F_2^\gamma(x, Q^2) = F_2^\gamma(x, Q^2)|_{light} + F_2^\gamma(x, Q^2)|_{heavy, FFNS} + F_2^\gamma(x, Q^2)|_{heavy, ZVFNS}, \quad (17)$$

would lead to double counting of some contributions. Let us notice first that the ZVFNS subprocess with the direct coupling of the real photon to the (massless) heavy quark, term  $C_{2,\gamma}^{(0)}(x)$  in Eq. (16), was also included in the FFNS formula (9) as  $C_{2,\gamma}^{h,(0)}(x, \frac{Q^2}{m_h^2})$ . Those two terms originate from the same  $\gamma^* + \gamma \rightarrow h + \bar{h}$  process, however they are not equal as the  $C_{2,\gamma}^{(0)}(x)$  term is obtained in a massless approximation. The same is true for the  $C_{2,G}^{(0)}(x)$  (Eq. (16)) and  $C_{2,G}^{h,(0)}(x, \frac{Q^2}{m_h^2})$  (Eq. (9)) terms arising from the  $\gamma^* + G \rightarrow h + \bar{h}$  process. Obviously, only one set of the above terms should be included in the final CJK NLO formula for the  $F_2^\gamma(x, Q^2)$ . We choose to apply the massive  $C_{2,\gamma}^{h,(0)}(x, \frac{Q^2}{m_h^2})$  and  $C_{2,G}^{h,(0)}(x, \frac{Q^2}{m_h^2})$  formulae, as unlike the massless approximations those terms properly vanish at the heavy-quark threshold.

The  $C_{2,q}^{(1)}$  coefficient in Eq. (16) is related with the process  $\gamma^* + h^\gamma \rightarrow h + G$ , with a heavy quark in the initial state and therefore appears only in the ZVFNS approach. It is the only heavy-quark Wilson coefficient which we apply in the massless approximation.

The massless  $C_{2,\gamma}^{(0)}(x)$  and  $C_{2,G}^{(0)}(x)$  terms are not the only ones that must be subtracted. Still, we double count the corresponding collinear configurations which are a part of the DGLAP equations and manifest themselves via the splitting functions  $P_{ij}$  and  $k_i$ . Such configurations give rise to terms proportional to  $\ln Q^2$  and through DGLAP equations are part of the heavy-quark densities  $q_h^\gamma(x, Q^2)$ . The same collinear configurations appear in massive heavy-quark Wilson coefficients  $C_{2,j}^{h,(n)}$ . Therefore, we must subtract the overlapping contributions. In the case of our model, where we neglect the higher order heavy-quark Wilson coefficients, there are only two such terms, same as in the LO case described in [1] and [2]. They are related to the  $\gamma^* + \gamma \rightarrow h + \bar{h}$  and  $\gamma^* + G \rightarrow h + \bar{h}$  processes. We calculate the necessary subtraction terms from the approximated integration of the corresponding parts of the DGLAP equations (7) and (8) over the region  $(Q_0^2, Q^2)$  (see [2]). The integration produces the  $\ln \frac{Q^2}{Q_0^2} \cdot e_h^2 \frac{\alpha}{2\pi} k_q^{(0)}(x)$  and  $\ln \frac{Q^2}{Q_0^2} \cdot \frac{\alpha_s(Q^2)}{2\pi} \int_{\chi_h}^1 \frac{dy}{y} P_{qG}^{(0)}(\frac{x}{y}) G(y, Q^2)$  terms<sup>3</sup>. These terms multiplied by  $2x$  and  $e_h^2$ , according to the formula  $F_2^\gamma(x, Q^2) = \sum_q x e_i^2 (q^\gamma + \bar{q}^\gamma)(x, Q^2)$ , must be subtracted from the sum of Eq. (17).

The described summation and subtraction procedure leads to the following formula

---

<sup>3</sup>Notice that we neglected the  $Q^2$  dependence of the strong coupling  $\alpha_s$  and the gluon density  $G(y, Q^2)$ .

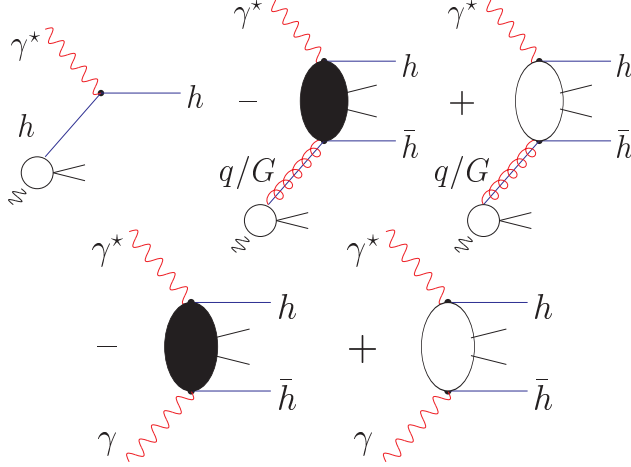


Figure 3: Graphical representation of the contributions to the CJK NLO model. The first diagram represents the ZVFNS contribution. The third and fifth diagrams show the FFNS resolved-photon and direct-photon contributions, respectively. The second and forth diagrams are the corresponding subtraction terms.

for the  $F_2^\gamma(x, Q^2)$  :

$$\begin{aligned}
 \frac{1}{x} F_2^\gamma(x, Q^2) = & \sum_{i=1}^3 e_i^2 \left\{ (q_i^\gamma + \bar{q}_i^\gamma)(x, Q^2) + e_i^2 \frac{\alpha}{2\pi} C_{2,\gamma}^{(0)}(x) \right. \\
 & + \frac{\alpha_s(Q^2)}{2\pi} \int_x^1 \frac{dy}{y} \left[ (q_i^\gamma + \bar{q}_i^\gamma)(y, Q^2) C_{2,q}^{(1)}\left(\frac{x}{y}\right) + G^\gamma(y, Q^2) C_{2,G}^{(1)}\left(\frac{x}{y}\right) \right] \left. \right\} \\
 & + \sum_{h(c,b)}^2 e_h^2 \left\{ (q_h^\gamma + \bar{q}_h^\gamma)(x, Q^2) + e_h^2 \frac{\alpha}{2\pi} C_{2,\gamma}^{h,(0)}(x, \frac{Q^2}{m_h^2}) \right. \\
 & + \frac{\alpha_s(Q^2)}{2\pi} \left[ \int_x^1 \frac{dy}{y} (q_h^\gamma + \bar{q}_h^\gamma)(y, Q^2) C_{2,q}^{(1)}\left(\frac{x}{y}\right) + \int_{x_h}^1 \frac{dy}{y} G^\gamma(y, Q^2) C_{2,G}^{h,(1)}\left(\frac{x}{y}, \frac{Q^2}{m_h^2}\right) \right] \\
 & \left. - \ln \frac{Q^2}{Q_0^2} \cdot 2e_h^2 \frac{\alpha}{2\pi} k_q^{(0)}(x) - \ln \frac{Q^2}{Q_0^2} \cdot 2 \frac{\alpha_s(Q^2)}{2\pi} \int_x^1 \frac{dy}{y} G^\gamma(y, Q^2) P_{qG}^{(0)}\left(\frac{x}{y}\right) \right\}. \tag{18}
 \end{aligned}$$

Its graphical representation is given in Fig. 3. If one includes the  $O(\alpha_s^2)$  and  $O(\alpha\alpha_s)$  heavy-quark contributions, the structure of the subtraction terms becomes more complicated, since one has to subtract terms proportional to  $k_q^{(1)}(x)$ ,  $P_{qG}^{(1)}(x)$  and  $P_{qq}^{(1)}(x)$ . Moreover these functions are divergent at  $x = 1$  and therefore their integrals lead to numerical instabilities. Solution of that problem is beyond the scope of this work.

#### 4.4 The $\overline{\text{MS}}$ and $\text{DIS}_\gamma$ factorization schemes

The introduction of the heavy-quark contributions to the  $F_2^\gamma(x, Q^2)$  forces us to apply a modified  $\text{DIS}_\gamma$  scheme in the CJK NLO model case. Let us recall that in this model apart from the massless, divergent at  $x \rightarrow 1$  contribution of light-quarks,  $C_{2,\gamma}^{(0)}(x)$ , the

massive, finite  $C_{2,\gamma}^{h,(0)}(x, \frac{Q^2}{m_h^2})$  term appears as the analogous heavy-quark contribution.

In order to remove the large- $x$  divergence of the  $C_{2,\gamma}^{(0)}(x)$  we proceed in the same way as described in the FFNS approach, absorbing that term into the light-quark distribution functions  $q_i^\gamma(x, Q^2)$ . What about the massive  $C_{2,\gamma}^{h,(0)}(x, \frac{Q^2}{m_h^2})$  contribution and the heavy-quark densities? The charm- and beauty-quark distributions in the CJK NLO model appear as a part of the massless ZVFNS scheme. The evolution of all partons is performed through the common set of five-flavour DGLAP evolution equations. Therefore, the subtraction of the  $C_{2,\gamma}^{(0)}(x)$  term from the Eq. (18) and modification of the  $k_{q_i}$  and  $k_G$  splitting functions (expressed in Eq. (13)) affect the heavy-quark densities in the same way as they affect the light-quark distributions. Namely, the following redefinition occurs:

$$\begin{aligned} q_h^{\text{DIS}_\gamma}(x, Q^2) &= q_h^{\overline{\text{MS}}}(x, Q^2) + e_h^2 \frac{\alpha}{4\pi} C_{2,\gamma}^{(0),\overline{\text{MS}}}(x), \\ C_{2,\gamma}^{h,(0),\text{DIS}_\gamma}(x, \frac{Q^2}{m_h^2}) &= C_{2,\gamma}^{h,(0),\overline{\text{MS}}}(x, \frac{Q^2}{m_h^2}) + \Delta C_{2,\gamma}^{(0)}(x). \end{aligned} \quad (19)$$

As  $\Delta C_{2,\gamma}^{(0)}(x) = -C_{2,\gamma}^{(0),\overline{\text{MS}}}(x)$ , see Eq. (12), the last equality takes form

$$C_{2,\gamma}^{h,(0),\text{DIS}_\gamma}(x, \frac{Q^2}{m_h^2}) = C_{2,\gamma}^{h,(0),\overline{\text{MS}}}(x, \frac{Q^2}{m_h^2}) - C_{2,\gamma}^{(0),\overline{\text{MS}}}(x). \quad (20)$$

In practice the subtraction of Eq. (20) can not be performed in such a simple way. Again, the  $C_{2,\gamma}^{(0),\overline{\text{MS}}}(x)$  term on the right side would lead to a divergence at large  $x$  and the advantage of the  $\text{DIS}_\gamma$  scheme would be lost. We have to proceed in a different way.

We decide to resolve the above problem by loosing part of the information brought by the massive  $C_{2,\gamma}^{h,(0),\overline{\text{MS}}}(x)$  contribution. That term calculated in the  $m_h^2 \approx 0$  approximation leads to (see Appendix A)

$$\begin{aligned} C_{2,\gamma}^{h,(0),\overline{\text{MS}}}(x, \frac{Q^2}{m_h^2}) &= C_{2,\gamma}^{(0),\overline{\text{MS}}}(x) + e_h^4 2k_q^{(0),\overline{\text{MS}}}(x) \ln \frac{Q^2}{m_h^2} \\ &+ 6e_h^4 \left[ -\beta x(1-x) \frac{4m_h^2}{Q^2} + \left( x(1-3x) \frac{4m_h^2}{Q^2} - x^2 \frac{8m_h^4}{Q^4} \right) \ln \frac{1+\beta}{1-\beta} \right], \end{aligned} \quad (21)$$

where we keep the heavy-quark mass and  $\beta = \sqrt{1 - \frac{4m_h^2 x}{(1-x)Q^2}}$  wherever it is possible. Let us notice now that the term  $\sim k_q^{(0),\overline{\text{MS}}}(x)$  of Eq. (21) differs from the first subtraction term in Eq. (18) only by the constant  $\sim \ln \frac{m_h^2}{Q_0^2}$ . We omit that constant and obtain in the  $\overline{\text{MS}}$  scheme:

$$\begin{aligned} C_{2,\gamma}^{h,(0),\overline{\text{MS}}}(x, \frac{Q^2}{m_h^2}) - \ln \frac{Q^2}{Q_0^2} \cdot 2e_h^4 k_q^{(0),\overline{\text{MS}}}(x) &\approx \\ \approx C_{2,\gamma}^{(0),\overline{\text{MS}}}(x) + 6e_h^4 \left[ -\beta x(1-x) \frac{4m_h^2}{Q^2} + \left( x(1-3x) \frac{4m_h^2}{Q^2} - x^2 \frac{8m_h^4}{Q^4} \right) \ln \frac{1+\beta}{1-\beta} \right], \end{aligned} \quad (22)$$

which according to Eq. (20) leads to the following relation in the  $\text{DIS}_\gamma$  scheme

$$\begin{aligned} & \frac{\alpha}{2\pi} C_{2,\gamma}^{h,(0),\text{DIS}_\gamma}(x, \frac{Q^2}{m_h^2}) - \ln \frac{Q^2}{Q_0^2} \cdot 2e_h^4 \frac{\alpha}{2\pi} k_q^{(0),\overline{\text{MS}}}(x) \approx \\ & \approx 3e_h^4 \frac{\alpha}{\pi} \left[ -\beta x(1-x) \frac{4m_h^2}{Q^2} + \left( x(1-3x) \frac{4m_h^2}{Q^2} - x^2 \frac{8m_h^4}{Q^4} \right) \ln \frac{1+\beta}{1-\beta} \right]. \end{aligned} \quad (23)$$

In the following we use only the  $\text{DIS}_\gamma$  factorization scheme, and omit the superscript for simplicity.

## 4.5 The $\chi_h$ variables

Let us recall that VFNS schemes widely utilize an approach in which  $q_h^\gamma(x, Q^2) = 0$  for all  $Q^2$  values smaller than  $m_h^2$  and  $q_h^\gamma(x, Q^2)$  becomes nonzero for  $Q^2 \geq m_h^2$ . At each such step the number of active quarks grows by one. This approach leads to unphysical heavy-quark densities near their production thresholds. The kinematical threshold of the heavy-quark production, and therefore its non-zero density in the photon, is given in  $\text{DIS}_{e\gamma}$  by the total energy of the  $e\gamma^*$  process,  $W$ . As discussed in section 2  $W$  must be greater than the sum of two masses of the heavy quark in hand,  $W > 2m_h$ .  $W$  and  $Q^2$  are connected,  $W^2 = (1-x)Q^2/x$ , which is the reason why the ZVFNS condition  $Q^2 \geq m_h^2$  for treating the heavy quark  $h$  as a parton is too simple.

In the  $\text{ACOT}(\chi)$  scheme used by the CJK NLO model the number of active quarks is equal  $N_f = 5$  at the whole range of the DGLAP evolution. To ensure that a heavy-quark,  $q_h^\gamma(x, Q^2)$ , distribution disappears when  $W \rightarrow 2m_h$  one introduces a new variable  $\chi_h \equiv x(1 + 4m_h^2/Q^2)$  and calculates  $q_h^\gamma(\chi_h, Q^2)$  in place of the  $q_h^\gamma(x, Q^2)$ . At the threshold, when  $W = 2m_h$ , we obtain  $\chi_h = 1$  and the corresponding heavy-quark density vanishes as desired. The form of the  $\chi_h$  variables could be chosen differently if only their above threshold behaviour was preserved. We chose to apply the same form as appears in the integration of the massive heavy-quark Wilson coefficients with the parton distributions, see also [4]. That way the same variable takes care of the proper vanishing of the  $h$ -quark density and of the  $\sim \int_{\chi_h}^1 \frac{dy}{y} G^\gamma(y, Q^2) C_{2,G}^{h,(1)}(\frac{x}{y}, \frac{Q^2}{m_h^2})$  contribution to  $F_2^\gamma(x, Q^2)$  at the kinematic limit. For the consistency of the approach also in the subtraction  $\sim \int_x^1 \frac{dy}{y} P_{qG}^{(0)}(\frac{x}{y}) G^\gamma(y, Q^2)$  term we exchange  $x$  with  $\chi_h$  and that way enforce its proper kinematic behaviour.

As described in [1] and [2] the subtraction  $\sim k_q^{(0)}(x)$  term does not vanish as  $W \rightarrow 2m_h$  even when one replaces  $x$  with  $\chi_h$ . In the NLO case we avoid that problem because, as discussed in section 4.4, that contribution cancels in the modified  $\text{DIS}_\gamma$  factorization scheme.

Unfortunately, a particular heavy-quark contribution appears in the NLO analysis which causes new problems at the threshold. The contribution  $\sim \int_x^1 \frac{dy}{y} (q_h^\gamma + \bar{q}_h^\gamma)(y, Q^2) C_{2,q}^{(1)}(\frac{x}{y})$  from the ZVFNS scheme could be rewritten in two ways, as  $\sim \int_{\chi_h}^1 \frac{dy}{y} (q_h^\gamma + \bar{q}_h^\gamma)(y, Q^2) C_{2,q}^{(1)}(\frac{x}{y})$  or as  $\sim \int_x^1 \frac{dy}{y} (q_h^\gamma + \bar{q}_h^\gamma)(\gamma_h, Q^2) C_{2,q}^{(1)}(\frac{x}{y})$ , with  $\gamma_h$  defined analogically to  $\chi_h$  ( $\gamma_h = y(1 + 4m_h^2/Q^2)$ ). The first approach leads to numerical instabilities for  $y$  values close to  $x$  originating from the  $\frac{1+x^2}{1-x} \ln \frac{1-x}{x}$  term in  $C_{2,q}^{(1)}(\frac{x}{y})$ . Second

form can not be adopted for the technical reasons in the Mellin space. Therefore, we use the unmodified formula of Eq. (18). Finally, to avoid the non-zero heavy-quark contributions in the kinematically forbidden  $(x, Q^2)$  region we impose by hand the following constraint:  $\int_x^1 \frac{dy}{y} (q_h + \bar{q}_h)(y, Q^2) C_{2,q}^{(1)}(\frac{x}{y}) = 0$  for  $\chi_h > 1$ . Obviously, the same reasoning would apply to higher order  $C_{2,q}^{(j)}$  coefficients neglected in the CJK NLO model.

## 4.6 Formula for $F_2^\gamma$

Summing the light- and heavy-quark contributions, converting them into the DIS $_\gamma$  factorization scheme and finally introducing the  $\chi_h$  variables we obtain the final formula of the  $F_2^\gamma(x, Q^2)$  in the CJK NLO model:

$$\begin{aligned} \frac{1}{x} F_2^\gamma(x, Q^2) = & \sum_{i=1}^3 e_i^2 \left\{ (q_i^\gamma + \bar{q}_i^\gamma)(x, Q^2) + \frac{\alpha_s(Q^2)}{2\pi} \int_x^1 \frac{dy}{y} \left[ (q_i^\gamma + \bar{q}_i^\gamma)(y, Q^2) C_{2,q}^{(1)}\left(\frac{x}{y}\right) + G^\gamma(y, Q^2) C_{2,G}^{(1)}\left(\frac{x}{y}\right) \right] \right\} \\ & + \sum_{h=1}^2 e_h^2 \left\{ (q_h^\gamma + \bar{q}_h^\gamma)(\chi_h, Q^2) + \frac{\alpha_s(Q^2)}{2\pi} \left[ \int_x^1 \frac{dy}{y} (q_h^\gamma + \bar{q}_h^\gamma)(y, Q^2) C_{2,q}^{(1)}\left(\frac{x}{y}\right) \right. \right. \\ & + \left. \left. \int_{\chi_h}^1 \frac{dy}{y} G^\gamma(y, Q^2) C_{2,G}^{h,(1)}\left(\frac{x}{y}, \frac{Q^2}{m_h^2}\right) - \ln \frac{Q^2}{Q_0^2} \cdot 2 \int_{\chi_h}^1 \frac{dy}{y} G^\gamma(y, Q^2) P_{qG}^{(0)}\left(\frac{\chi_h}{y}\right) \right] \right\} \\ & + 3e_h^2 \frac{\alpha}{\pi} \left[ -\beta x(1-x) \frac{4m_h^2}{Q^2} + \left( x(1-3x) \frac{4m_h^2}{Q^2} - x^2 \frac{8m_h^4}{Q^4} \right) \ln \frac{1+\beta}{1-\beta} \right]. \end{aligned} \quad (24)$$

To prevent the unphysical situation, in which the ZVFNS scheme contribution to  $F_2^\gamma(x, Q^2)$  is negative, or in other words in which the total  $F_2^\gamma(x, Q^2)$  is smaller than the FFNS scheme contribution, as in [1–3], separately for each heavy quark, we impose an additional positivity condition, here in form:

$$(q_h^\gamma + \bar{q}_h^\gamma)(\chi_h, Q^2) + \frac{\alpha_s}{2\pi} \left[ \int_x^1 \frac{dy}{y} (q_h^\gamma + \bar{q}_h^\gamma)(y, Q^2) C_{2,q}^{(1)}\left(\frac{x}{y}\right) - \ln \frac{Q^2}{Q_0^2} \cdot 2 \int_{\chi_h}^1 \frac{dy}{y} G^\gamma(y, Q^2) P_{qG}^{(0)}\left(\frac{\chi_h}{y}\right) \right] \geq 0. \quad (25)$$

## 5 Global fits - solving the DGLAP evolution

In this section the technical details of the solution of the DGLAP evolution equations are shortly described.

### 5.1 Mellin moments

The DGLAP evolution equations (7) and (8) as well as the structure function formulae (14) and (24) are very much simplified if they are transformed into the Mellin-moments space. The  $n$ -th moment, where  $n$  is a complex number, for any function  $f$ , generally depending on  $x$  and  $Q^2$  is defined by  $f^n(Q^2) = \int_0^1 x^{n-1} f(x, Q^2) dx$ . We apply

this definition to the parton distributions, splitting functions and the light-quark Wilson coefficients  $C_{2,i}^{(k)}(x)$ . Their convolution integrals in the  $(x, Q^2)$  space transform into multiplication of the corresponding moments in the Mellin space. This simple correspondence does not hold in the case of the convolutions with the heavy-quark Wilson coefficient  $C_{2,G}^{h,(1)}(x, \frac{Q^2}{m_h^2})$  and the  $P_{qG}^{(0)}(x)$  splitting function because of the integration limit  $\chi_h$ . Therefore those integrations must be performed in the  $(x, Q^2)$  space. All results calculated in the Mellin space are transformed through the inverse Mellin transformation to obtain their values in the  $(x, Q^2)$  space.

## 5.2 Nonsinglet and singlet parton densities

In the photon case we define the singlet ( $\Sigma^\gamma$ ) and non-singlet ( $f_{\text{NS}(N_f)}^\gamma(x, Q^2)$ ) quark distributions as

$$f_{\text{NS}(N_f)}^\gamma(x, Q^2) = \sum_{i=1}^{N_f} (e_i^2 - \langle e^2 \rangle) [q_i^\gamma(x, Q^2) + \bar{q}_i^\gamma(x, Q^2)], \quad (26)$$

$$\Sigma^\gamma(x, Q^2) = \sum_{i=1}^{N_f} [q_i^\gamma(x, Q^2) + \bar{q}_i^\gamma(x, Q^2)] \quad (27)$$

with

$$\langle e^k \rangle = N_f^{-1} \sum_{i=1}^{N_f} e_i^k. \quad (28)$$

For the singlet density we sum over all quark flavours appearing in the evolution, the active quarks,  $N_f = 5$ . Although in CJK model  $N_f = 5$ , for the non-singlet case it is necessary to calculate all,  $q_{\text{NS}(3)}^\gamma$ ,  $q_{\text{NS}(4)}^\gamma$  and  $q_{\text{NS}(5)}^\gamma(x, Q^2)$  to obtain all six parton distributions, see [1].

The evolution of the non-singlet distributions is governed by the simplified DGLAP equation. In the Mellin moments space it reads

$$\frac{df_{\text{NS}(N_f)}^{\gamma,n}(Q^2)}{d \ln Q^2} = \frac{\alpha}{2\pi} k_{\text{NS}(N_f)}^n + \frac{\alpha_s(Q^2)}{2\pi} P_{qq}^{\text{NS},n} f_{\text{NS}(N_f)}^{\gamma,n}(Q^2). \quad (29)$$

The singlet distribution evolution is coupled with the evolution of the gluon density

$$\frac{d\Sigma^{\gamma,n}(Q^2)}{d \ln Q^2} = \frac{\alpha}{2\pi} k_\Sigma^n + \frac{\alpha_s(Q^2)}{2\pi} \left[ P_{\Sigma\Sigma}^n \Sigma^{\gamma,n}(Q^2) + P_{\Sigma G}^n G^{\gamma,n}(Q^2) \right], \quad (30)$$

$$\frac{dG^{\gamma,n}(Q^2)}{d \ln Q^2} = \frac{\alpha}{2\pi} k_G^n + \frac{\alpha_s(Q^2)}{2\pi} \left[ P_{G\Sigma}^n \Sigma^{\gamma,n}(Q^2) + P_{GG}^n G^{\gamma,n}(Q^2) \right]. \quad (31)$$

Therefore, one has to solve the matrix equation

$$\frac{d\vec{f}_S^{\gamma,n}(Q^2)}{d \ln Q^2} = \frac{\alpha}{2\pi} \vec{k}_S^n + \frac{\alpha_s(Q^2)}{2\pi} \hat{P}^{S,n} f_S^{\gamma,n}(Q^2). \quad (32)$$

with

$$\vec{q}_S^{\gamma,n} = \begin{bmatrix} \Sigma^{\gamma,n} \\ G^{\gamma,n} \end{bmatrix}, \quad \vec{k}_S^n = \begin{bmatrix} k_\Sigma^n \\ k_G^n \end{bmatrix}, \quad \hat{P}^{S,n} = \begin{bmatrix} P_{\Sigma\Sigma}^n & P_{\Sigma G}^n \\ P_{G\Sigma}^n & P_{GG}^n \end{bmatrix}. \quad (33)$$

The new point-like splitting functions are defined as

$$\begin{aligned} k_{NS(N_f)}(x) &= 2N_f \left( \langle e^4 \rangle - \langle e^2 \rangle^2 \right) \left[ k_q^{(0)} + \frac{\alpha_s(Q^2)}{2\pi} k_q^{(1)} \right] (x), \\ k_\Sigma(x) &= 2N_f \langle e^2 \rangle \left[ k_q^{(0)} + \frac{\alpha_s(Q^2)}{2\pi} k_q^{(1)} \right] (x). \end{aligned} \quad (34)$$

The formulae for the above splitting functions  $P_{ij}(x, Q^2)$  can be found for instance in [15]. Their Mellin moments were calculated in [18].

### 5.3 Point- and hadron-like parts

The solution to the DGLAP equations can be divided into the so called point-like (pl) part, related to a special solution of the full inhomogenous equations and hadron-like (had) part, being a general solution of the homogenous equations. Their sum gives the parton density in the photon, so we have

$$f_{NS(N_f)}^{\gamma,n}(Q^2) = f_{NS(N_f),\text{had}}^{\gamma,n}(Q^2) + f_{NS(N_f),\text{pl}}^{\gamma,n}(Q^2), \quad (35)$$

$$\vec{f}_S^{\gamma,n}(Q^2) = \vec{f}_{S,\text{had}}^{\gamma,n}(Q^2) + \vec{f}_{S,\text{pl}}^{\gamma,n}(Q^2). \quad (36)$$

The non-singlet hadron-like solution is given as

$$q_{NS(N_f),\text{had}}^{\gamma,n}(Q^2) = L^{-2P_{qq}^{(0),n}/\beta_0} \left\{ 1 - \frac{\alpha_s(Q^2) - \alpha_s(Q_0^2)}{\pi\beta_0} \hat{R} \right\} q_{NS(N_f),\text{had}}^{\gamma,n}(Q_0^2) \quad (37)$$

and the non-singlet point-like solution is

$$q_{NS(N_f),\text{pl}}^{\gamma,n}(Q^2) = \frac{4\pi}{\alpha_s(Q^2)} \left[ 1 - L^{1-2P_{qq}^{(0),n}/\beta_0} \right] a^n + \left[ 1 - L^{-2P_{qq}^{(0),n}/\beta_0} \right] b^n, \quad (38)$$

with

$$a^n = \frac{\alpha}{2\pi\beta_0} \frac{k_{NS}^{(0),n}}{1 - 2P_{qq}^{(0),n}/\beta_0}, \quad b^n = -\frac{1}{P_{qq}^{(0),n}} \left[ 2\hat{R}a^n + \frac{\alpha}{2\pi} \hat{K} \right] \quad (39)$$

and

$$L = \frac{\alpha_s(Q^2)}{\alpha_s(Q_0^2)}, \quad \hat{R} = P_{NS}^{(1),n} - \frac{\beta_1}{2\beta_0} P_{qq}^{(0),n}, \quad \hat{K} = k_{NS}^{(1),n} - \frac{\beta_1}{2\beta_0} k_{NS}^{(0),n}. \quad (40)$$

Here  $\beta_0$  and  $\beta_1$  are the coefficients of the running strong coupling,  $\alpha_s$ , which we discuss in detail in section 5.5.

The singlet point- and hadron-like solutions have the same form but are more complicated than the corresponding non-singlet solutions. All formulae can be found for instance in [17].

## 5.4 Input parton densities. VMD

The hadron-like parts of the singlet and non-singlet densities, denoted in this section as  $f_{\text{had}}$ , need input distributions. For this purpose we utilize the Vector Meson Dominance (VMD) model [19], where

$$f_{\text{had}}^\gamma(x, Q_0^2) = \sum_V \frac{4\pi\alpha}{\hat{f}_V^2} f^V(x, Q_0^2), \quad (41)$$

with sum running over all light vector mesons (V) into which the photon can fluctuate. The parameters  $\hat{f}_V^2$  can be extracted from the experimental data on  $\Gamma(V \rightarrow e^+e^-)$  width. In practice we take into account the  $\rho^0$  meson while the contributions from the other mesons are accounted for via a parameter  $\kappa$

$$f_{\text{had}}^\gamma(x, Q_0^2) = \kappa \frac{4\pi\alpha}{\hat{f}_\rho^2} f^\rho(x, Q_0^2), \quad (42)$$

which is left as a free parameter in the fits.

We use the input densities of the  $\rho^0$  meson at low  $Q_0^2$  in the form of valence-like distributions both for the (light) quark ( $v^\rho$ ) and gluon ( $G^\rho$ ) densities. All sea-quark distributions (denoted by  $\zeta^\rho$ ) are neglected at the input scale. At this scale, the densities  $v^\rho$ ,  $G^\rho$  and  $\zeta^\rho$  are related, according to Eq. (42) to the corresponding densities for a photon, see below.

The  $v^\rho$  density is given by

$$v^\rho(x, Q_0^2) = \frac{1}{4}(u^{\rho+} + \bar{u}^{\rho-} + d^{\rho-} + \bar{d}^{\rho+})(x, Q_0^2), \quad (43)$$

where from the isospin symmetry

$$u^{\rho+}(x, Q_0^2) = \bar{u}^{\rho-}(x, Q_0^2) = d^{\rho-}(x, Q_0^2) = \bar{d}^{\rho+}(x, Q_0^2). \quad (44)$$

Note that all the densities in Eq. (43) are normalized to 1, eg.  $\int_0^1 u^{\rho+} dx = 1$ .

Two constraints should hold for the  $v^\rho(x, Q_0^2)$  density, the first one is related to a number of valence quarks in the  $\rho^0$  meson,

$$\int_0^1 2v^\rho(x, Q_0^2) dx = 2, \quad (45)$$

the second constraint represents the energy-momentum sum rule:

$$\int_0^1 x (2v^\rho(x, Q_0^2) + G^\rho(x, Q_0^2)) dx = 1. \quad (46)$$

We parametrize the input densities as follows:

$$\begin{aligned} x\zeta^\rho(x, Q_0^2) &= 0, \\ xv^\rho(x, Q_0^2) &= N_v x^\alpha (1-x)^\beta, \\ xG^\rho(x, Q_0^2) &= \tilde{N}_G x v^\rho(x, Q_0^2) = N_G x^\alpha (1-x)^\beta, \end{aligned} \quad (47)$$

where  $N_G = \tilde{N}_G N_v$ . Like in the LO analysis, [1–3], the input gluon distribution is proportional to the valence one and both have the valence-like form. Further, we impose two constraints given by Eqs. (45) and (46) in both types of models: FFNS<sub>CKJ</sub> and CJK NLO. These constraints allow us to express the normalization factors  $N_v$  and  $N_G$  as functions of  $\alpha, \beta$  and  $\kappa$ . This leaves these three parameters as the only free parameters to be fixed in the fits to the  $F_2^\gamma$  experimental data.

## 5.5 $\alpha_s$ running and values of $\Lambda^{(N_q)}$

We distinguish between the number of active quarks in the photon,  $N_f$ , and the number of quarks contributing to the running of  $\alpha_s$ , which we denote by  $N_q$ , [2]. The  $N_f$  depends only on the choice of the type of the model: ones we decide to use the FFNS<sub>CKJ</sub> or CJK NLO approach, then  $N_f = 3$  or  $5$ , respectively, through the whole  $Q^2$  range of evolution. On contrary  $N_q$  depends on the  $Q^2$  value. It is equal  $3$  when  $Q^2 < m_c^2$  and increases by one unit whenever  $Q^2$  reaches a heavy-quark threshold, i.e. when  $Q^2 = m_h^2$ .

The running of the strong coupling constant in NLO is given then by the well-known formula:

$$\frac{\alpha_s^{(N_q)}(Q^2)}{4\pi} = \frac{1}{\beta_0 \ln(Q^2/\Lambda^{(N_q)})^2} - \frac{\beta_1}{\beta_0^3} \frac{\ln \ln(Q^2/\Lambda^{(N_q)})^2}{(\Lambda^{(N_q)})^2} \quad (48)$$

with

$$\beta_0 = 11 - \frac{2}{3}N_q, \quad \beta_1 = 102 - \frac{38}{3}N_q. \quad (49)$$

For  $N_q = 4$  we took the QCD scale  $\Lambda^{(4)}$  equal to  $280$  MeV [22]. In order to ensure the continuity of the strong coupling constant at the heavy-quark thresholds the condition  $\alpha_s^{(N_q)}(m_h^2) = \alpha_s^{(N_q+1)}(m_h^2)$  is imposed. We calculate values of the remaining  $\Lambda^{(N_q)}$  constants according to the above condition. We utilizing the relation between constants  $\Lambda^{(N_q)}$  and  $\Lambda^{(N_q+1)}$  given in [21]. That way we obtain  $\Lambda^{(3)} = 0.323$  MeV and  $\Lambda^{(5)} = 0.200$  MeV.

The parton evolution equations depend on  $N_q$  through their dependence on  $\alpha_s(Q^2)$  and independently  $\beta_0$  and  $\beta_1$ , see Eqs. (37) and (38). Therefore, because of the implicit introduction of the heavy-quark thresholds into the  $\alpha_s$  running we must proceed in three steps to perform the DGLAP evolution. In the first step, describing the evolution from the input scale  $Q_0$  to the charm-quark mass  $m_c$ , the hadronic input  $q_{\text{had}}^\gamma(x, Q_0^2)$  is taken from the VMD model. In the second step we evolve the parton distributions from  $m_c$  to the beauty-quark mass,  $m_b$ . Then, a new hadronic input is given by the sum of the already evolved hadronic and point-like contributions. The point-like distribution at  $Q^2 = m_c^2$  becomes zero again. The same is repeated for  $Q^2 > m_b^2$ .

## 6 Global fits - results

We have performed a series of fits to the  $F_2^\gamma(x, Q^2)$  data [23]–[36]. All together 192 data points were used, including the recent results of the ALEPH Collaboration [34], which replaced the old preliminary data [38], as well as recent preliminary results of the

DELPHI Collaboration [31] replacing the old preliminary data [37]. In that case only the LEP1 data were applied because no final results for the LEP2 data are given in a form useful for our global fits<sup>4</sup> in [31]. Our fits based on the least square principle (minimum of  $\chi^2$ ) were done using MINUIT [42]. Systematic and statistical errors of data points were added in quadrature.

First, we made two test fits in which, following the analysis of the GRS group, [8], we assumed the input scale value  $Q_0^2 = 0.4 \text{ GeV}^2$ . The results of both fits are presented in table 3. The first two columns show the quality of the fits, i.e. the total  $\chi^2$  for 192 points and the  $\chi^2$  per degree of freedom. The fitted values for parameters  $\alpha$ ,  $\beta$  and  $\kappa$  are presented in the middle of the table with the symmetric parabolic errors obtained from MIGRAD requiring  $\Delta\chi^2 = 1$ <sup>5</sup>. In addition, the values for  $N_v$  and  $\tilde{N}_G$  obtained from these parameters, using the constraints (45) and (46), are given in the last two columns. As can be seen the fits give high  $\chi^2$  per degree of freedom. Further, the relatively small  $\kappa$  value indicates respectively small contribution of heavier mesons which is compensated by a very high, especially in case of the CJK NLO model, valence-quark input ( $N_v = 9.26$ ).

NLO models	$\chi^2$	$\chi^2/DOF$	$\kappa$	$\alpha$	$\beta$	$N_v$	$\tilde{N}_G$
FFNS <sub>CJK1</sub>	318.0	1.68	$1.40 \pm 0.06$	$1.15 \pm 0.16$	$1.24 \pm 0.42$	2.80	0.949
CJK	299.9	1.51	$1.40 \pm 0.05$	$1.38 \pm 0.18$	$3.40 \pm 0.77$	9.26	2.19

Table 3: The  $\chi^2$  and parameters of the test fits for 192 data points for FFNS<sub>CJK1</sub> NLO and CJK NLO models with assumed  $Q_0^2 = 0.4 \text{ GeV}^2$ . The  $\alpha$ ,  $\beta$  and  $\kappa$  symmetric parabolic errors obtained from MIGRAD requiring  $\Delta\chi^2 = 1$ .

In order to obtain better agreement with the data two other fits were performed, in which  $Q_0^2$  was treated at first as a free parameter. For both models we obtained very similar  $Q_0^2 \approx 0.765 \text{ GeV}^2$  ( $Q_0 = 0.875 \text{ GeV}$ ) values. Therefore in our final CJK and FFNS<sub>CJK</sub>-NLO fits we fixed the input scale as  $Q_0^2 = 0.765 \text{ GeV}^2$ . The  $Q_0 = 0.875 \text{ GeV}$  value agrees with the  $Q_0 = 0.85 \pm 0.09 \text{ GeV}$  obtained in the recent NLO fit presented in [10]. The results of both CJK and FFNS<sub>CJK1</sub> NLO fits are presented in table 4. The errors shown in the table were obtained from MINOS requiring  $\Delta\chi^2 = 1$ .

As expected, estimation of the  $Q_0^2$  value through the test fits, allowed us to find sets of parameters which give better agreement of both models with the data. We use these sets as the final results of our analysis. Comparison of the  $\chi^2/DOF$  values obtained in the test and final fits shows the  $\sim 0.40$  and  $\sim 0.30$  improvement in the FFNS<sub>CJK1</sub> and CJK NLO models respectively. Further, in both cases we observe an increase of the  $\kappa$  parameter with the simultaneous decrease of  $\alpha$ ,  $\beta$  and  $N_v$ . That change can be explained by the fact that in higher  $Q^2$  valence distribution broadens (change of  $\alpha$ ,  $\beta$ ) but at the same time the constraint (45) maintains its integral constant. Finally,

<sup>4</sup>All LEP2 data are given in three sets obtained with the TWOGAM [39], PHOJET [40] and PYTHIA [41] Monte Carlo generators.

<sup>5</sup>For test fits we applied MIGRAD instead of MINOS which requires much more computer time

the  $\tilde{N}_G$  parameter grows at higher  $Q_0^2$  because the gluon contribution to the photon structure increases with the increasing  $Q^2$ .

The choice of the  $F_2^\gamma(x, Q^2)$  distributions predicted by the test and final fits are presented in Figs. 4 and 5 for the FFNS<sub>CJK1</sub> and CJK NLO models, respectively. As the main difference we observe faster growth of the  $F_2^\gamma$  function at small  $x$  in the case of the test fits with  $Q_0^2 = 0.4$  GeV<sup>2</sup>, especially at small  $Q^2$ . The medium and high- $x$  predictions for the photon structure function are similar apart from the low  $Q^2$  region.

NLO models	$\chi^2$	$\chi^2/DOF$	$\kappa$	$\alpha$	$\beta$	$N_v$	$\tilde{N}_G$
FFNS <sub>CJK1</sub>	243.3	1.29	$2.288^{+0.108}_{-0.096}$	$0.502^{+0.071}_{-0.066}$	$0.690^{+0.282}_{-0.252}$	0.685	2.369
CJK	256.8	1.37	$2.662^{+0.108}_{-0.099}$	$0.496^{+0.063}_{-0.057}$	$1.013^{+0.284}_{-0.255}$	0.745	3.056

Table 4: The  $\chi^2$  and parameters of the final fits for 192 data points for FFNS<sub>CJK1</sub> NLO and CJK NLO models with assumed  $Q_0^2 = 0.765$  GeV<sup>2</sup>. The  $\alpha$ ,  $\beta$  and  $\kappa$  errors obtained from MINOS requiring  $\Delta\chi^2 = 1$ .

Moreover, we see that unlike in the LO case (see [1] and [2]), and in the case of the test fits with  $Q_0^2 = 0.4$  GeV<sup>2</sup>, the obtained  $\chi^2$  per degree of freedom is better in the standard type FFNS model than in the CJK model. The origin of the relatively high  $\chi^2/DOF$  in both fits comparing to much lower  $\chi^2 \approx 0.9$  obtained in [10] is the same as in the LO case, discussed in detail in [3]. Namely, the exclusion of the CELLO [23] and recent DELPHI [31] data from the fits leads to much better agreement among fits and the data.

Further, we performed test fits with the modified set of the input densities (47). Namely, we used the input gluon distribution independent of the valence one

$$\begin{aligned} x\zeta^\rho(x, Q_0^2) &= 0, \\ xv^\rho(x, Q_0^2) &= N_v x^\alpha (1-x)^\beta, \\ xG^\rho(x, Q_0^2) &= N_G x^{\alpha_G} (1-x)^{\beta_G}. \end{aligned} \quad (50)$$

Fits gave very high values of the  $\alpha_G$  and  $\beta_G$  parameters, around 14 and 16 respectively, leading to fast oscillations of the input gluon densities and all parton densities at low  $Q^2$ . The  $N_G$  parameter calculated using constraint (46) is of the order  $10^9$ . Moreover, the  $\alpha_G$  and  $\beta_G$  values have very high uncertainties and therefore it is hard to obtain the final convergence of the fits. Taking all this and the fact that the  $\chi^2/DOF$  values obtained in the test fits are slightly higher than the once presented above, we conclude that the choice of the simple form of the input distributions of Eqs. (47) is very reasonable even at  $Q_0^2 \approx 0.8$  GeV<sup>2</sup>.

## 6.1 Comparison of the CJK and FFNS<sub>CJK</sub> NLO fits with $F_2^\gamma$ data and other NLO parametrizations

Figures 6–9 show a comparison of the CJK and FFNS<sub>CJK1</sub> NLO fits to  $F_2^\gamma(x, Q^2)$  with the experimental data as a function of  $x$ , for different values of  $Q^2$ . Also a comparison

with the GRS NLO [8] and AFG NLO [43] parametrizations is shown. (If a few values of  $Q^2$  are displayed in a panel, the average of the smallest and biggest one was taken in the computation.) As can be seen in Figs. 6 and 7, both CJK and FFNS<sub>CKJ1</sub> NLO models predict a much steeper behaviour of the  $F_2^\gamma(x, Q^2)$  at small  $x$  with respect to other parametrizations. In the region of medium and high  $x$ , the behaviour of the  $F_2^\gamma(x, Q^2)$  obtained from the FFNS<sub>CKJ1</sub> and CJK NLO fits is similar to the one computed with the GRS NLO parametrization while it is very different to the AFG parametrization prediction, see Figs. 8 and 9. Below the charm-quark threshold the CJK model gives the highest  $F_2^\gamma$  and the GRS NLO parametrization the lowest  $F_2^\gamma$  of the three similar predictions while above the threshold that order is inverted. Finally, at high  $Q^2$  and high  $x$  the  $F_2^\gamma$  computed in the FFNS<sub>CKJ1</sub> NLO model and GRS NLO parametrization become undistinguishable while the CJK NLO prediction is visibly larger.

Next, in Figs. 10 and 11 we compare the CJK and FFNS<sub>CKJ1</sub> NLO fits with the corresponding CJK and FFNS<sub>CKJ2</sub> LO fits presented in [2]. Figure 10 shows very small differences, only in the low  $x$  region the FFNS<sub>CKJ1</sub> NLO model gives greater values than other models and parametrizations. On the other hand, as it can be seen in Fig. 11, the NLO models predict higher  $F_2^\gamma$  than the LO ones at the  $x$  region right below the charm-quark threshold. Moreover the NLO predictions vanish more rapidly at  $x \rightarrow 1$ .

Apart from the direct comparison with the photon structure-function data, we perform another comparison, this time with LEP data that were not used directly in our analysis. Figures 12 and 13 present the predictions for  $F_2^\gamma(x, Q^2)$ , averaged over various  $x$  regions, compared with the recent OPAL data [36]. For comparison, the results from the GRS and AFG NLO parametrizations are shown as well. In Fig. 12 we observe that in the medium- $x$  range,  $0.1 < x < 0.6$ , all models give expectations of the same shape, all in fairly good agreement with the experimental data. Still, in small  $Q^2$  the  $F_2^\gamma$  computed with the AFG NLO parametrization is above the others, and starting at approximately  $Q^2 = 3$  GeV $^2$  the predictions of the GRS NLO parametrization are lower than the other three. In the  $x$  ranges presented in Fig. 13 we also notice many differences among the averaged  $F_2^\gamma(x, Q^2)$  predictions computed in various models. The only exception give the FFNS<sub>CKJ1</sub> NLO and the GRS NLO predictions which are very close to each other in the whole  $Q^2$  range and in all, apart from the lowest,  $x$  ranges examined. Let us now name all the dissimilarities observed in Fig. 13. Firstly, the  $F_2^\gamma(Q^2)$  predicted by the CJK NLO model shows clear change of the behaviour in the high  $Q^2$  and high  $x$  range where we observe its larger increase than predicted by the other models. Secondly, the expectations of the AFG parametrization in the same regions (also for small  $Q^2$ ) lie much below the other results. Finally, the GRS NLO parametrization predicts slightly lower  $F_2^\gamma(Q^2)$  values than the remaining models.

## 6.2 Parton densities

In this section we present the parton densities obtained from the CJK and FFNS<sub>CKJ1</sub> NLO fits and compare them with the corresponding distributions of the GRV [7], GRS and AFG NLO parametrizations. First, we present all parton densities at  $Q^2 = 10$

GeV<sup>2</sup> (Fig. 14). The biggest difference between our CJK NLO model and others is observed, as expected, for the heavy-quark distributions. Unlike for the GRV and AFG NLO parametrizations (there is no beauty-quark density in the AFG NLO parametrization), our  $c^\gamma(x, Q^2)$  and  $b^\gamma(x, Q^2)$  densities vanish not at  $x = 1$  but, as it should be, at the kinematical threshold. Moreover, we notice a huge difference between the beauty-quark distributions computed in two models. The GRV NLO parametrization predicts the  $b^\gamma(x, Q^2)$  values of the same order as the  $c^\gamma(x, Q^2)$ . In Fig. 17, where the charm-quark distributions are presented for various  $Q^2$  values, apart from different threshold behaviour we observe that CJK  $c^\gamma(x, Q^2)$  distribution is the largest of all down to very small  $x$  value (depending on  $Q^2$ ) where the GRV density becomes larger. The light-quark and gluon densities calculated in our models and the GRV and GRS NLO parametrizations generally have the same shapes but their values differ. Main differences are observed in the up-, down-quark and gluon distributions. The  $u^\gamma$  densities computed in both our models are lower than in other parametrizations at high  $x$ . In the Fig. 15 we see differences among predictions of all models at very low  $x$ . Still we do not find a general pattern of those distinctions. In the case of the gluon distribution, see Figs. 14 and 16, we observe that at all  $Q^2$  regions the CJK model gives the largest predictions. At high  $Q^2$ ,  $G^\gamma(x, Q^2)$  calculated in the FFNS<sub>CKJ1</sub> NLO model and in GRV NLO parametrization become similar. The GRS and AFG NLO predictions lie below all other lines in the whole  $x$  and  $Q^2$  range.

Further, we compare our CJK and FFNS<sub>CKJ1</sub> NLO parton distributions with the corresponding CJK and FFNS<sub>CKJ2</sub> LO ones. As can be seen in Fig. 18, for  $Q^2 = 10$  GeV<sup>2</sup>, the NLO models predict higher up- and down-quark densities in the medium- $x$  region and steeper increase of the gluon distribution. The growth of  $G^\gamma(x, Q^2)$  at low  $x$  is especially fast in the CJK NLO model case while the FFNS<sub>CKJ1</sub> NLO model prediction tends to fuse with the LO ones. Moreover, all NLO quark densities vanish more rapidly at  $x \rightarrow 1$  than the LO quark densities.

### 6.3 Comparison with $F_{2,c}^\gamma$

In Fig. 19 we present the CJK NLO predictions for the  $F_{2,c}^\gamma$ . For  $Q^2 = 5, 20, 100$  and 1000 GeV<sup>2</sup> we compare the individual contributions included in the model. Analogically to the LO case, see [1] and [2], we introduce the following notation

$$F_{2,c}^\gamma(x, Q^2) = 2xe_c^2 c^\gamma(x, Q^2) + F_{2,c}^\gamma|_{\text{dir}}(x, Q^2) + F_{2,c}^\gamma|_{\text{res}}(x, Q^2) - F_{2,c}^\gamma|_{\text{res,sub}}(x, Q^2) + \left[ 2c * C_{2,q}^{(1)} \right] (x, Q^2) \quad (51)$$

with

$$\begin{aligned}
F_{2,c}^\gamma|_{\text{dir}}(x, Q^2) &= 3e_c^2 \frac{\alpha}{\pi} \left[ -\beta x(1-x) \frac{4m_c^2}{Q^2} + \left( x(1-3x) \frac{4m_c^2}{Q^2} - x^2 \frac{8m_c^4}{Q^4} \right) \ln \frac{1+\beta}{1-\beta} \right], \\
F_{2,c}^\gamma|_{\text{res}}(x, Q^2) &= \int_{\chi_c}^1 \frac{dy}{y} G^\gamma(y, Q^2) C_{2,G}^{h,(1)}\left(\frac{x}{y}, \frac{Q^2}{m_c^2}\right), \\
F_{2,c}^\gamma|_{\text{res,sub}}(x, Q^2) &= \ln \frac{Q^2}{Q_0^2} \cdot 2 \int_{\chi_c}^1 \frac{dy}{y} G^\gamma(y, Q^2) P_{qG}^{(0)}\left(\frac{\chi_c}{y}\right), \\
[2c * C_{2,q}^{(1)}](x, Q^2) &= \int_x^1 \frac{dy}{y} (c^\gamma + \bar{c}^\gamma)(y, Q^2) C_{2,q}^{(1)}\left(\frac{x}{y}\right).
\end{aligned} \tag{52}$$

Let us stress that the above direct contribution effectively includes both the direct and direct subtraction terms, as discussed in detail in section 4.4. Therefore, it is not the same as the  $F_{2,c}^\gamma|_{\text{dir}}(x, Q^2)$  in the LO analyses. That way in the NLO analysis we removed the troublesome subtraction term  $\sim k_q^{(0)}$ . Unfortunately, also the  $2c * C_{2,q}^{(1)}$  contribution does not vanish at the threshold and therefore an additional constraint  $2c * C_{2,q}^{(1)} = 0$  for  $\chi_c > 1$  is necessary. This term is important in the high and medium  $x$ , its values in the latter range are negative. As can be seen in the plot all other terms vanish in the  $W \rightarrow 2m_c$  threshold. The direct term influences the  $F_{2,c}^\gamma$  only in the midium and high  $x$  at low- $Q^2$  range, where it is negative. The charm-quark density contribution, i.e. the term  $2xe_c^2 c^\gamma(x, Q^2)$ , dominates the  $F_{2,c}^\gamma$  in the whole kinematically available  $x$  range. In the low- $x$  region also the resolved-photon contributions increase, but they cancel each other.

A good test of the charm-quark contributions is provided by the OPAL measurement of the  $F_{2,c}^\gamma$ , obtained from the inclusive production of  $D^{*\pm}$  mesons in the photon–photon collisions [44]. The averaged  $F_{2,c}^\gamma$  has been determined in the two  $x$  bins. These data points are compared to the predictions of the CJK and FFNS<sub>CJK1</sub> NLO models, as well as of the corresponding CJK and FFNS<sub>CJK2</sub> LO models in Fig. 20. The CJK NLO model seems to give the best description of the data, especially for the high- $x$  bin. The FFNS type models predict the same  $F_{2,c}^\gamma$  at  $x > 0.03$ , while below that value the FFNS<sub>CJK2</sub> LO predicts higher  $F_{2,c}^\gamma$  which finally becomes very similar to the NLO results.

## 6.4 Test of importance of $O(\alpha_s^2)$ and $O(\alpha\alpha_s)$ terms

In this section we would like to present the results of the fit of the FFNS<sub>CJK2</sub> NLO model to the data. As discussed in Sections 3.2 and 3.4, in this approach we include the  $O(\alpha_s^2)$  and  $O(\alpha\alpha_s)$  contributions to the photon structure function:

$$\begin{aligned}
\frac{1}{x} F_2^\gamma(x, Q^2)|_{\text{higher order}} &= \\
\sum_{h=c,b}^2 \left\{ \left( \frac{\alpha_s(Q^2)}{2\pi} \right)^2 \int_{\chi_h}^1 \frac{dy}{y} \left[ \sum_{i=1}^3 (q_i^\gamma + \bar{q}_i^\gamma)(y, Q^2) (e_i^2 C_{2,q}^{(2)}\left(\frac{x}{y}, \frac{Q^2}{m_h^2}\right) + e_h^2 C_{2,q}^{h,(2)}\left(\frac{x}{y}, \frac{Q^2}{m_h^2}\right)) \right. \right. \\
&\quad \left. \left. + e_h^2 G^\gamma(y, Q^2) C_{2,G}^{h,(2)}\left(\frac{x}{y}, \frac{Q^2}{m_h^2}\right) \right] + \frac{\alpha\alpha_s(Q^2)}{(2\pi)^2} e_h^4 C_{2,\gamma}^{h,(1)}(x, \frac{Q^2}{m_h^2}) \right\}.
\end{aligned} \tag{53}$$

Alike in the main CJK and  $\text{FFNS}_{CJK1}$  NLO models our fit was performed in two steps. First, we treated  $Q_0^2$  as a free parameter in order to obtain better agreement with the data, next it was fixed to the estimated value,  $Q_0^2 = 0.716 \text{ GeV}^2$ , and a final fit was done. Its results are presented in table 5, all errors were obtained from MINOS requiring  $\Delta\chi^2 = 1$ .

NLO model	$\chi^2$	$\chi^2/DOF$	$\kappa$	$\alpha$	$\beta$	$N_v$	$\tilde{N}_G$
$\text{FFNS}_{CJK2}$	252.2	1.31	$1.892^{+0.101}_{-0.090}$	$0.527^{+0.089}_{-0.080}$	$0.966^{+0.387}_{-0.333}$	0.797	2.727

Table 5: The  $\chi^2$  and parameters of the fit for the  $\text{FFNS}_{CJK2}$  NLO model with assumed  $Q_0^2 = 0.716 \text{ GeV}^2$ . The  $\alpha$ ,  $\beta$  and  $\kappa$  symmetric parabolic errors obtained from MINOS requiring  $\Delta\chi^2 = 1$ .

First let us compare the results of the two  $\text{FFNS}_{CJK}$  NLO models, given in tables 4 and 5, respectively. We notice that higher  $\chi^2/DOF$  is obtained in the model including additional terms. Next, the input scale and the parameters obtained in both approaches are very similar. Largest distinction is observed between the  $\kappa$  values and can be explained by the small difference between the  $Q_0^2$  values (0.716 and 0.786  $\text{GeV}^2$ , respectively). Namely, when we start the evolution of the parton densities at lower input scale then smaller input distributions are required in order to obtain the same results at the given  $Q^2$ .

Further, we compare results computed using four various  $\text{FFNS}_{CJK}$  models, the NLO ones described in this work as well as the  $\text{FFNS}_{CJK1} \& 2$  LO models, presented in [2]. The main differences among the four models, apart from the different order of the QCD DGLAP equations applied, lie in the heavy-quark contributions to  $F_2^\gamma$ . Those differences are summarized in table 6 where all included or discluded terms proportional to Wilson-coefficient functions are listed.

$\text{FFNS}_{CJK}$ model	$C_{2,\gamma}^{h,(0)}$	$C_{2,G}^{h,(1)}$	$C_{2,\gamma}^{h,(1)}$	$C_{2,G}^{h,(2)}$	$C_{2,q}^{h,(2)}$	$C_{2,q}^{(2)}$
LO 1	+	-	-	-	-	-
LO 2	+	+	-	-	-	-
NLO 1	+	+	-	-	-	-
NLO 2	+	+	+	+	+	+

Table 6: The heavy-quark terms proportional to the Wilson coefficient functions contributing (or not) to the heavy-quark structure function in various  $\text{FFNS}_{CJK}$  models.

In Fig. 21 we compare the parton densities computed in the  $\text{FFNS}_{CJK}$  models obtained in LO and NLO. We observe that two LO models predict nearly the same parton distributions which begin to differ in the very low- $x$  region (the larger differences at  $x$  below 0.1 are not shown). The distinctions between the pairs of LO and NLO lines

are large at high  $x$  where, as discussed before, the NLO distributions decrease much earlier. The maximal values of the NLO  $u^\gamma$  and  $s^\gamma$  distributions are reached at smaller  $x$ ,  $x \sim 0.75$  than in the LO case where the corresponding  $x$  value is  $x \sim 0.95$ . Moreover, there exist important differences between the two NLO fits, observed especially in the up- and down-quark distributions, which indicate the importance of the higher order  $O(\alpha_s^2)$  and  $O(\alpha\alpha_s)$  contributions to  $F_2^\gamma(x, Q^2)$  at medium  $x$ . Smaller difference between the LO results seen in Fig. 21 may be explained by the fact that in that case the models differ only by the resolved-type  $\sim C_{2,G}^{h,(1)}$  contribution, which plays important role only in the low- $x$  region. Very similar conclusion may be drawn from the comparison of the  $F_2^\gamma(x, Q^2)$  distributions plotted in Figs. 22 and 23. Alike in the parton densities case the LO  $F_2^\gamma(x, Q^2)$  distributions differ only in the very low- $x$  region, see Fig. 23, while the NLO ones mostly at high  $x$ .

## 6.5 Influence of the DELPHI LEP2 data

Finally we tested the possible influence of the recent DELPHI data [31], which were not included in the final fits, on the results of our models. We performed test fits for the CJK NLO model including separately each of the sets of the LEP2 data obtained with TWOGAM [39], PHOJET [40] and PYTHIA [41] Monte Carlo generators and presented in [31]. As can be seen in Figs. 24 and 25 for the choice of the  $F_2^\gamma(x, Q^2)$  distributions and the parton densities computed at  $Q^2 = 10$  GeV $^2$ , respectively, the results of that fits are very similar to the expectations of the final CJK NLO fit (denoted as “no LEP2”). Still, the  $\chi^2/DOF$  obtained in the test fits are much worse, see table 7.

set	$\chi^2$	# of points	$\chi^2/DOF$
TWOGAM	307.4	209	1.50
PHOJET	312.0	207	1.54
PYTHIA	341.1	209	1.66

Table 7: Number of experimental points used in the test fits for the CJK NLO model and the resulting  $\chi^2$ .

## 7 Discussion and conclusions

A new analysis of the radiatively generated parton distributions in the real photon based on the NLO DGLAP equations is presented. An updated set of the  $F_2^\gamma(x, Q^2)$  data including recent ALEPH as well as new preliminary DELPHI measurements has been used to perform three global fits. Our models base on two schemes, the Fixed Flavour-Number Scheme and Variable Flavour-Number Scheme (ACOT( $\chi$ )) which were already applied in our former LO analysis, see [1]- [3]. We observe that in comparison to the LO models higher input scale of the NLO DGLAP evolution is required

in order to satisfactorily describe the data. Further, unlike in the LO case we obtained lower  $\chi^2/DOF$  in the FFNS type approach than in the CJK model. The test fits showed that a change of the simple form of the input parton distributions applied in [1–3] and in this work does not lead to the improvement of the fits.

Predictions of the  $FFNS_{CJK1}$  and CJK NLO fits are compared with the  $F_2^\gamma(x, Q^2)$  data, other parametrizations and corresponding LO models. Both models describe very well the  $Q^2$  evolution of the  $F_2^\gamma(x, Q^2)$ , averaged over various  $x$ -regions. The  $F_{2,c}^\gamma$  calculated in the CJK NLO model gives best agreement with the data.

Next, we check the difference between the results obtained in the  $FFNS_{CJK1}$  NLO model and the  $FFNS_{CJK2}$  NLO model which includes additional  $O(\alpha_s^2)$  and  $O(\alpha\alpha_s)$  contributions to  $F_2^\gamma(x, Q^2)$ . Those higher order terms prove to be of importance. Therefore, further studies of the CJK model including terms of the same order are required.

Finally, we examine the influence on the results of our models of the various sets of the LEP2 data presented in the recent preliminary results of the DELPHI Collaboration but discluded from final fits. Test fits show very small change of the  $F_2^\gamma(x, Q^2)$  and parton distributions obtained using these data comparing to the final fits but large deterioration of their quality.

Fortran parametrization programs for our CJK and  $FFNS_{CJK}$  NLO models can be obtained from the web-page [45].

## Acknowledgements

P.J. would like to thank E.Laenen for making accessible the formulae for the Wilson coefficients and for his comments. Moreover, P.J. is grateful to I.Schienbein for his help in obtaining correct NLO DGLAP evolution programs. We want to thank R.Gokieli and K.Doroba for their comments on the recent DELPHI data. Finally P.J. is grateful to M.Aurenche and M.Fontannaz for the AFG parametrization program, R.Nisius for all his remarks concerning the experimental data and A.Zembrzuski for his comments.

This work was partly supported by the European Community's Human Potential Programme under contract HPRN-CT-2000-00149 Physics at Collider and HPRN-CT-2002-00311 EURIDICE. FC also acknowledges partial financial support from Ministerio de Ciencia y Tecnología under project FPA2003-09298-c02-01 and Junta de Andalucía under project FQM 330. This work was partially supported by the Polish Committee for Scientific Research, grant no. 1 P03B 040 26 and project no. 115/E-343/SPB/DESY/P-03/DWM517/2003-2005.

## Appendix: The Wilson-coefficient functions

Lists of all Wilson-coefficient functions used in this analysis are given in tables 1 and 2. The Wilson coefficients  $C_{2,q}^{(1)}$ ,  $C_{2,G}^{(1)}$  and  $C_{2,\gamma}^{(0)}$  have been first calculated in the operator product expansion [46] in the Mellin space in the articles [47] and [48], respectively. In

the  $(x, Q^2)$  space the  $C_{2,\gamma}^{(1)}$  in the  $\overline{\text{MS}}$  factorization scheme reads (see for instance [8])

$$C_{2,\gamma}^{(1)}(x) = 6 \left[ -1 + 8x(1-x) + (x^2 + (1-x)^2) \ln \frac{1-x}{x} \right]. \quad (54)$$

The lowest order heavy-quark coefficient  $C_{2,\gamma}^{h,(0)}$ , given by the Bethe-Heitler  $\gamma^* + \gamma \rightarrow q + \bar{q}$  process, has been first presented in [49]. It has the following form:

$$\begin{aligned} C_{2,\gamma}^{h,(0)}(x, \frac{Q^2}{m_h^2}) &= 6 \frac{\alpha}{\pi} e_h^4 \beta \left[ -1 + 8x(1-x) - x(1-x) \frac{4m_h^2}{Q^2} \right] \\ &\quad + \ln \left( \frac{1+\beta}{1-\beta} \right) \left[ x^2 + (1-x)^2 + x(1-3x) \frac{4m_h^2}{Q^2} - x^2 \frac{8m_h^4}{Q^4} \right], \end{aligned} \quad (55)$$

$$\text{with } \beta = \sqrt{1 - \frac{4m_h^2 x}{(1-x)Q^2}}.$$

When we neglect the heavy-quark mass in some parts of the coefficient  $C_{2,\gamma}^{h,(0)}$  we can rewrite it as in Eq. (21)

$$\begin{aligned} C_{2,\gamma}^{h,(0),\overline{\text{MS}}}(x, \frac{Q^2}{m_h^2}) &\approx C_{2,\gamma}^{(0),\overline{\text{MS}}}(x) + e_h^4 2k_q^{(0),\overline{\text{MS}}}(x) \ln \frac{Q^2}{m_h^2} \\ &\quad + 6e_h^4 \left[ -\beta x(1-x) \frac{4m_h^2}{Q^2} + \left( x(1-3x) \frac{4m_h^2}{Q^2} - x^2 \frac{8m_h^4}{Q^4} \right) \ln \frac{1+\beta}{1-\beta} \right], \end{aligned} \quad (56)$$

where the direct photon-quark splitting function is

$$k_q^{(0)} = 3[x^2 + (1-x)^2]. \quad (57)$$

The  $C_{2,G}^{h,(1)}$  function related to the  $\gamma^* + G \rightarrow q + \bar{q}$  process reads

$$\begin{aligned} C_{2,G}^{h,(1)}(x, \frac{Q^2}{m_h^2}) &= \frac{1}{6} C_{2,\gamma}^{h,(0)}(x, \frac{Q^2}{m_h^2}) \\ &= \frac{\alpha}{\pi} e_h^4 \beta \left[ -1 + 8x(1-x) - x(1-x) \frac{4m_h^2}{Q^2} \right] \\ &\quad + \ln \left( \frac{1+\beta}{1-\beta} \right) \left[ x^2 + (1-x)^2 + x(1-3x) \frac{4m_h^2}{Q^2} - x^2 \frac{8m_h^4}{Q^4} \right]. \end{aligned} \quad (58)$$

Finally, the higher order heavy-quark coefficients,  $C_{2,\gamma}^{h,(1)}$ ,  $C_{2,G}^{(2)}$ ,  $C_{2,q}^{h,(2)}$  and  $C_{2,q}^{(2)}$  are calculated in the serious of publications [13]. They are given in the form of a two dimensional array. Those  $O(\alpha_s^2)$  and  $O(\alpha\alpha_s)$  order Wilson coefficients are given as

$$C_{2,i}^{h,(k)}(x, m_h^2, Q^2, \mu^2) = C_{2,i}^{h,(k)}(x, \frac{Q^2}{m_h^2}) + \bar{C}_{2,i}^{h,(k)}(x, \frac{Q^2}{m_h^2}) \ln \frac{\mu^2}{m_h^2}, \quad (59)$$

where  $\mu^2$  is the mass factorization scale. In our calculations we simplify the above formula by choosing  $\mu^2 = m_h^2$ .

## References

- [1] F.Cornet, P.Jankowski, M.Krawczyk and A.Lorca, Phys. Rev. **D68** 014010 (2003)
- [2] F.Cornet, P.Jankowski and M.Krawczyk, IFT-2003-30; F. Cornet, P.Jankowski and M.Krawczyk, *Contributed to Photon 2003: International Conference on the Structure and Interactions of the Photon and 15th International Workshop on Photon-Photon Collisions, Frascati, Italy, 7-11 Apr 2003*, hep-ph/0310029.
- [3] P.Jankowski, IFT-2003-31, hep-ph/0312056, accepted by JHEP
- [4] S.Kretzer, C.Schmidt and W.Tung, *Proceedings of New Trends in HERA Physics*, Ringberg Castle, Tegernsee, Germany, 17-22 Jun 2001, Published in J. Phys. **G28**, 983 (2002); S.Kretzer, H.L.Lai, F.I.Olness and W.K.Tung, hep-ph/0307022
- [5] M.Glück, E.Reya and A.Vogt, Z. Phys. **C53**, 127 (1992)
- [6] M.Glück, E.Reya and A.Vogt, Z. Phys. **C53**, 651 (1992)
- [7] M.Glück, E.Reya and A.Vogt, Phys. Rev. **D46**, 1973 (1992)
- [8] M.Glück, E.Reya and I.Schienbein, Phys. Rev. **D60**, 054019 (1999), Erratum-ibid. **D62**, 019902 (2000)
- [9] M.Glück, E.Reya and M.Stratmann, Phys. Rev. **D51**, 3220 (1995)
- [10] S.Albino, M.Klasen and S.Söldner-Rembold, Phys. Rev. Lett. **89**, 122004 (2002)
- [11] A.Chuvakin, J.Smith and W.L. van Neerven, Phys. Rev. **D61**, 096004 (2000)
- [12] A.Chuvakin, J.Smith and W.L. van Neerven, Phys. Rev. **D62**, 036004 (2000)
- [13] E.Laenen, S.Riemersma, J.Smith and W.L. van Neerven, Nucl. Phys. **B392**, 162 (1993); Phys. Lett. **B291**, 325 (1992); Phys. Rev. **D49**, 5753 (1994); S.Riemersma, J.Smith and W.L. van Neerven, Phys. Lett. **B347**, 143 (1995)
- [14] G. Parisi, Proceedings of 11th Rencontres de Moriond 1976, editor J. Tran Thanh Van, G. Altarelli and G. Parisi, Nucl. Phys. **B126**, 298 (1997).
- [15] R.K. Ellis, W.J. Stirling and B.R.Weber 'QCD and Collider Physics' (Cambridge University Press, 1996)
- [16] M.Glück, E.Reya and A.Vogt, Phys. Rev. **D45**, 3986 (1992)
- [17] A.Vogt, "The Partonic structure of hadrons and photons," Ph.D. Thesis, Dortmund University, May 1992; DO-TH-92-15
- [18] E.G. Floratos, C. Kounnas and R. Lacaze, Nucl. Phys. **B192**, 417 (1981)
- [19] J.H. Field, VIIIth International Workshop on Photon-Photon Collisions, Shoresh, Jerusalem Hills Israel, 1988; U. Maor, Acta Phys. Polonica **B19**, 623 (1988); Ch. Berger and W. Wagner, Phys. Rep. **146**, 1 (1987)

- [20] B. L. Ioffe, hep-ph/0209254
- [21] J.C. Collins and W. Tung, Nucl. Phys. **B278**, 934 (1986)
- [22] By Particle data Group (D.E.Groom *et al.*), Eur. Phys. J. **C15**, 1 (2000)
- [23] CELLO Collaboration, H.J.Behrend *et al.*, Phys. Lett. **B126**, 391 (1983); in *Proceedings of the XXVth International Conference on High Energy Physics*, Singapore, 1990, edited by K.K.Phua and Y.Yamaguchi (World Scientific, Singapore, 1991)
- [24] PLUTO Collaboration, Ch.Berger *et al.*, Phys. Lett. **B142** 111 (1984); Nucl. Phys. **B281**, 365 (1987)
- [25] JADE Collaboration, W.Bartel *et al.*, Z. Phys. **C24**, 231 (1984)
- [26] TPC/2 $\gamma$  Collaboration, H.Aihara *et al.*, Z. Phys. **C34**, 1 (1987); J.S.Steinman, Ph.D. Thesis, UCLA-HEP-88-004, Jul 1988
- [27] TASSO Collaboration, M.Althoff *et al.*, Z.Phys **C31**, 527 (1986)
- [28] TOPAZ Collaboration, K.Muramatsu *et al.*, Phys.Lett. **B332**, 477 (1994)
- [29] AMY Collaboration, S.K.Sahu *et al.*, Phys. Lett. **B346**, 208 (1995); T.Kojima *et al.*, *ibid.* **B400**, 395 (1997)
- [30] DELPHI Collaboration, P.Abreu *et al.*, Z. Phys. **C69**, 223 (1996); I.Tyapkin, *Proceedings of Workshop on Photon Interaction and the Photon Structure*, Lund, Sweden, Sept. 1998, edited by G.Jarlskog and T.Sjöstrand
- [31] DELPHI Collaboration, Contributed Paper for *European Physical Society International Europhysics Conference on High Energy Physics* 17-23 July, 2003, Aachen, Germany and *Lepton Photon 2003 XXI International Symposium on Lepton and Photon Interactions at High Energies* 11-16 August, 2003, Fermilab, Batavia, Illinois USA
- [32] L3 Collaboration, M.Acciarri *et al.*, Phys. Lett. **B436**, 403 (1998); *ibid.* **B447**, 147 (1999); *ibid.* **B483**, 373 (2000)
- [33] ALEPH Collaboration, R.Barate *et al.*, Phys. Lett. **B458**, 152 (1999)
- [34] ALEPH Collaboration, A. Heister *et al.*, Eur. Phys. J. **C30**, 145 (2003)
- [35] OPAL Collaboration, K.Ackerstaff *et al.*, Z. Phys. **C74**, 33 (1997); Phys. Lett. **B411**, 387 (1997); G.Abbiendi *et al.*, Eur. Phys. J. **C18**, 15 (2000)
- [36] OPAL Collaboration, G.Abbiendi *et al.*, Phys. Lett. **B533**, 207 (2002)

- [37] DELPHI Collaboration, I.Tyapkin, Published in the *Proceedings of International Conference on the Structure and Interactions of the Photon and 14th International Workshop on Photon-Photon Collisions (Photon 2001)*, Ascona, Switzerland, 2-7 Sep 2001
- [38] ALEPH Collaboration, K.Affholderbach *et al.*, *Proceedings of the International Europhysics Conference on High Energy Physics*, Tampere, Finland, 1999, Nucl. Phys. Proc. Suppl. **B86**, 122 (2000)
- [39] S.Nova, A.Olshevsky, T.Todorov, DELPHI-90-35 (unpublished)
- [40] Humboldt University, D-10099 Berlin, FRG
- [41] Workshop on Physics at LEP2, CERN 96-01 v2 (1996)
- [42] F.James and M.Roos, Comput. Phys. Commun. **10**, 343 (1975)
- [43] P. Aurenche, J.-P. Guillet and M. Fontannaz, "Parton Distributions in the Photon", Z. Phys. **C64**, 621 (1994)
- [44] OPAL Collaboration, G.Abbiendi *et al.*, Phys. Lett. **B539**, 13 (2002)
- [45] <http://www.fuw.edu.pl/~pjank/param.html>
- [46] K.G. Wilson, Phys. Rev. **179**, 1499 (1969)
- [47] W. A. Bardeen, A. J. Buras, D. W. Duke and T. Muta, Phys. Rev. **D18**, 3998 (1978)
- [48] W. A. Bardeen and A. J. Buras, Phys. Rev. **D20**, 166 (1979) [Erratum-ibid. **D21**, 2041 (1980)]
- [49] E. Witten, Nucl. Phys. B **104**, 445 (1976); M. Glück and E. Reya, Phys. Lett. B **83**, 98 (1979)

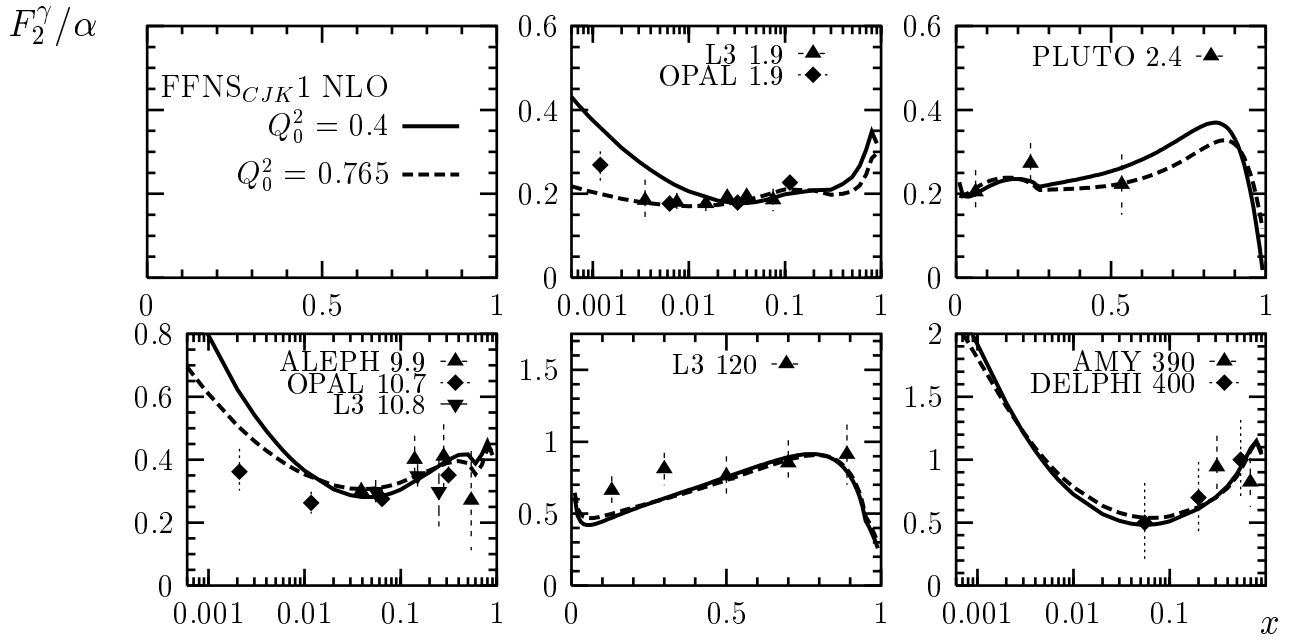


Figure 4: Predictions for the  $F_2^\gamma(x, Q^2)/\alpha$  for the  $FFNS_{CJK1}$  NLO model obtained by the main fit with  $Q_0^2 = 0.765$  GeV $^2$  and by the test fit with  $Q_0^2 = 0.4$  GeV $^2$ .

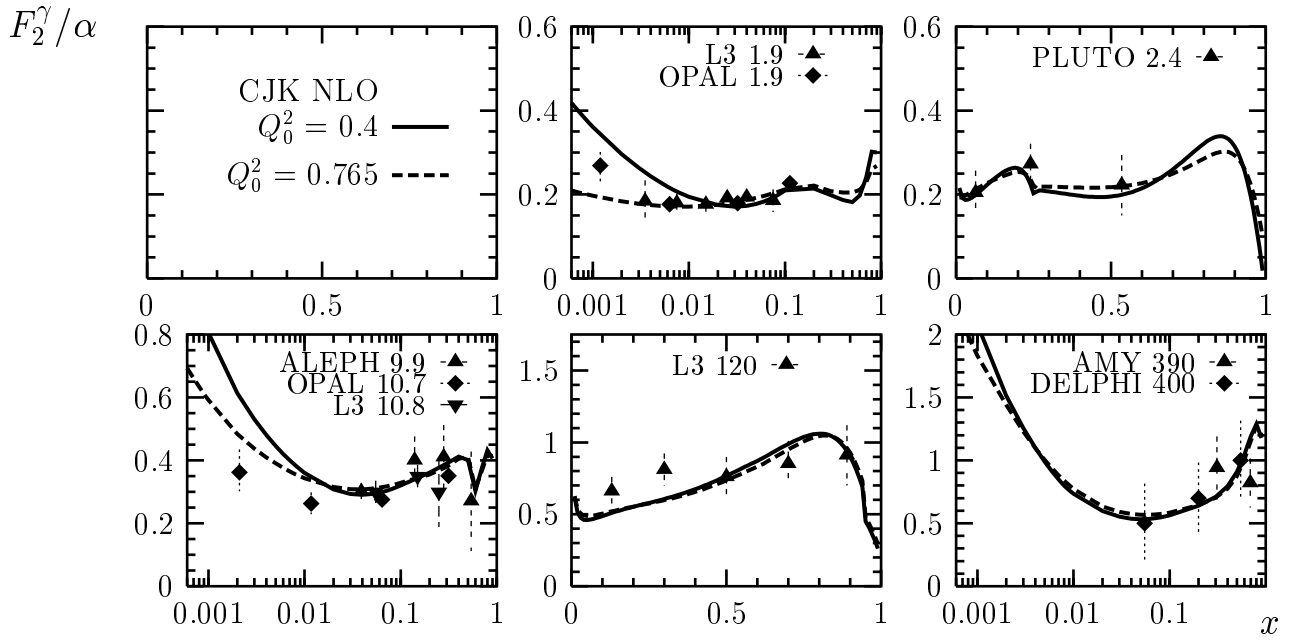


Figure 5: The same as in Fig. 4 for the CJK NLO model.

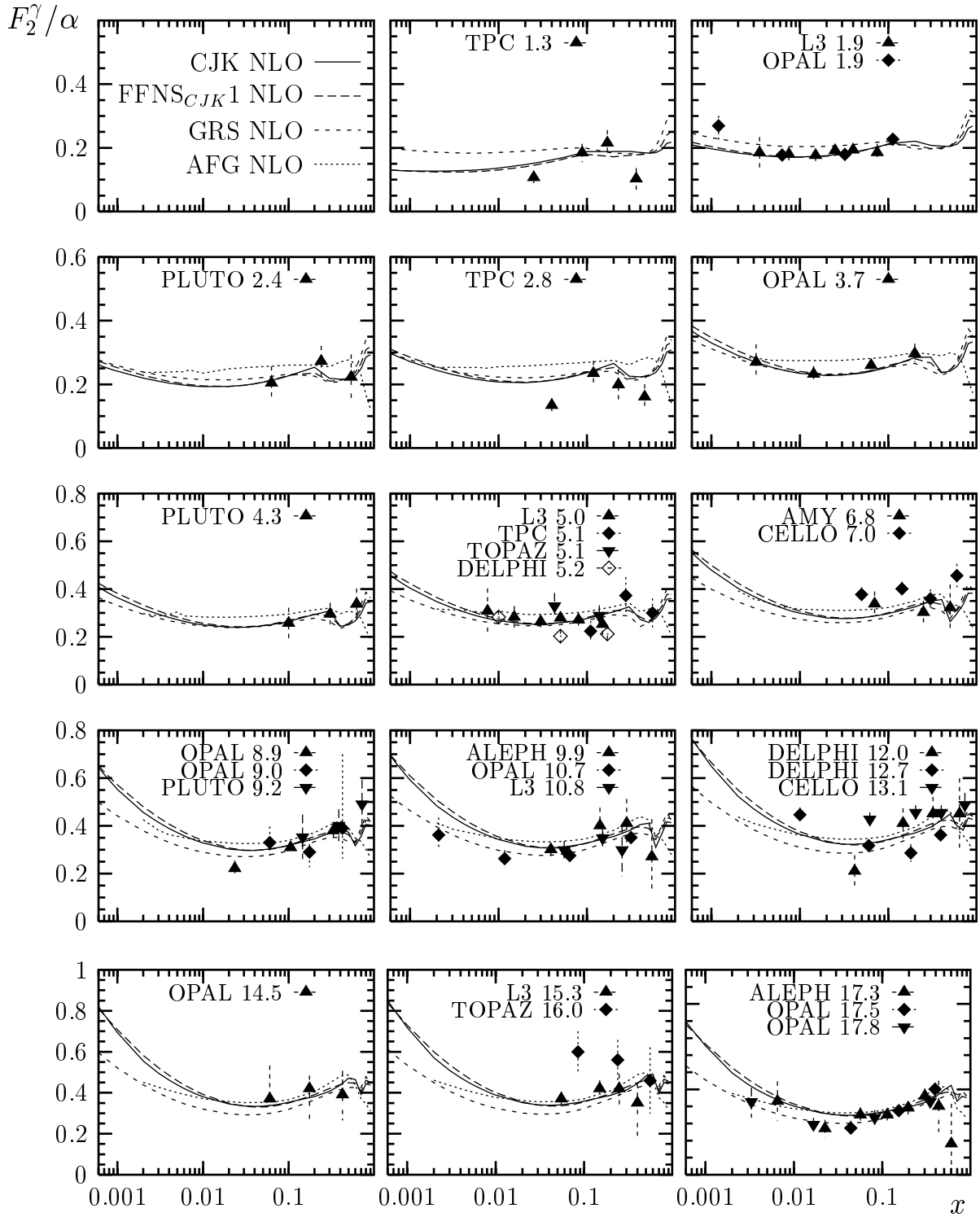


Figure 6: Predictions for the  $F_2^\gamma(x, Q^2)/\alpha$  for the CJK NLO and  $FFNS_{CJK1}$  NLO models and GRS NLO [8] and AFG NLO [43] compared with the experimental data [23]– [36], for small and medium  $Q^2$  as a function of  $x$  (logarithmic scale). If a few values of  $Q^2$  are displayed in the panel, the average of the smallest and biggest  $Q^2$  was taken in the computation.

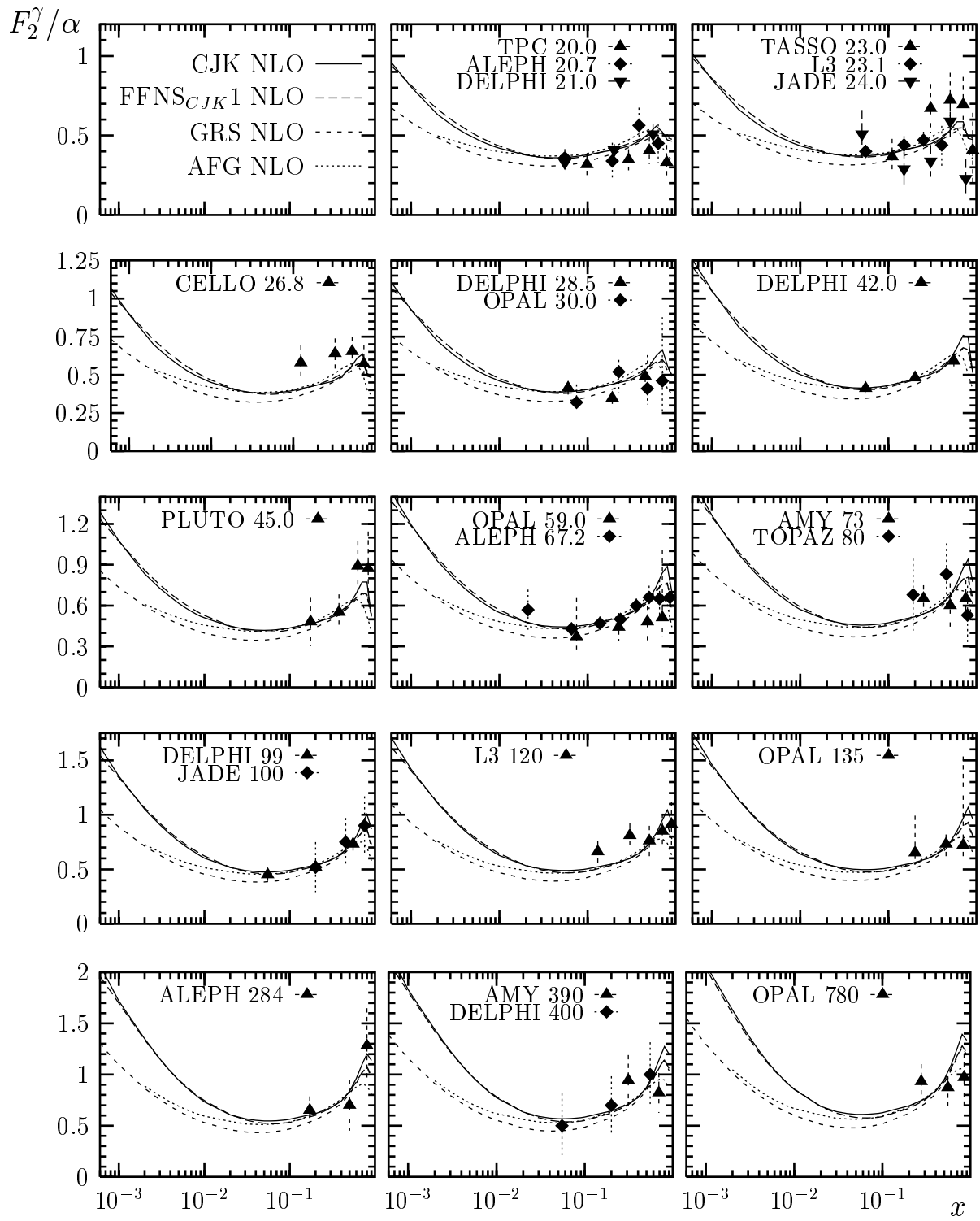


Figure 7: The same as in Fig. 6, for  $Q^2 \geq 20 \text{ GeV}^2$ .

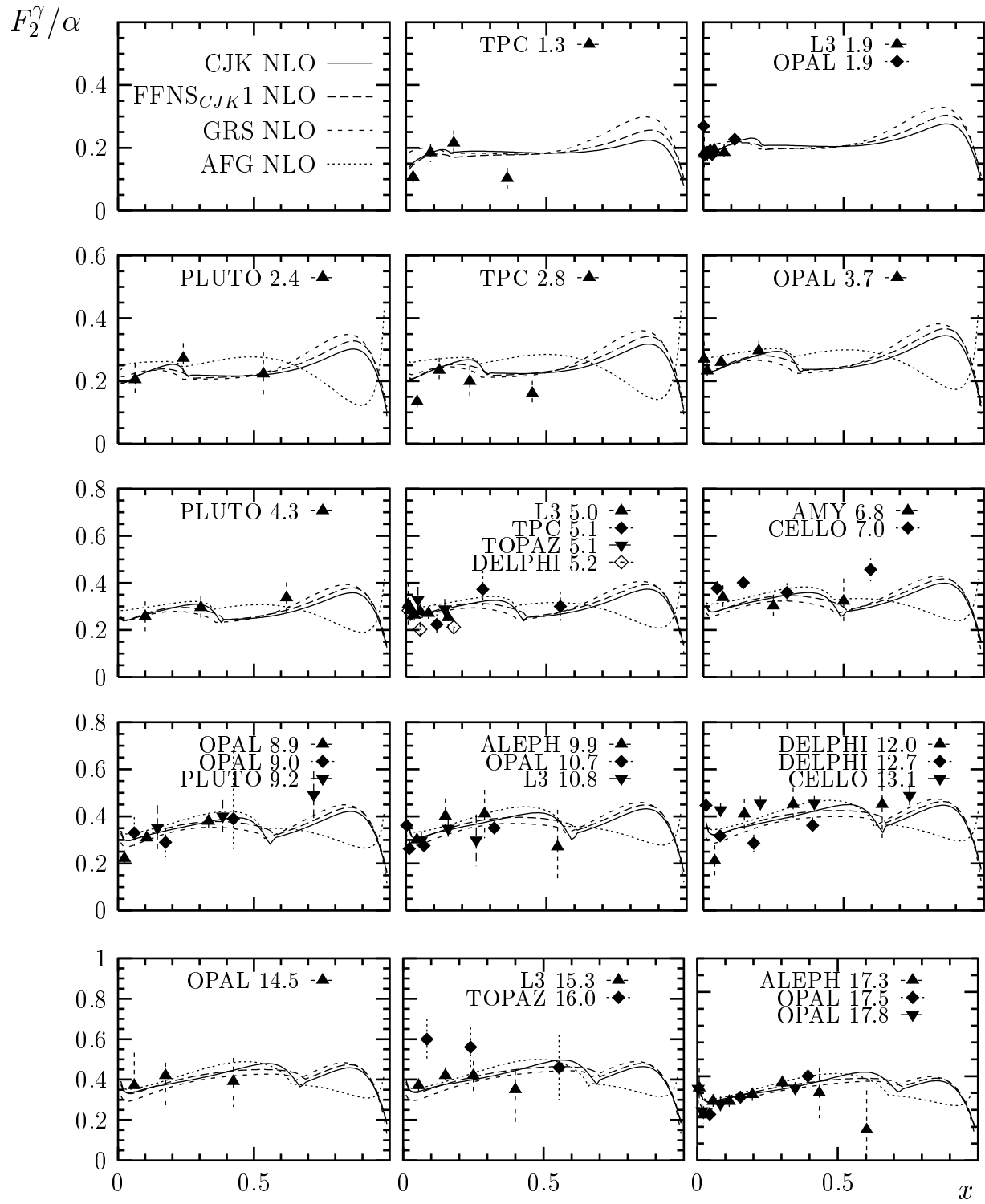


Figure 8: The same as in Fig. 6 for a linear scale in  $x$ .

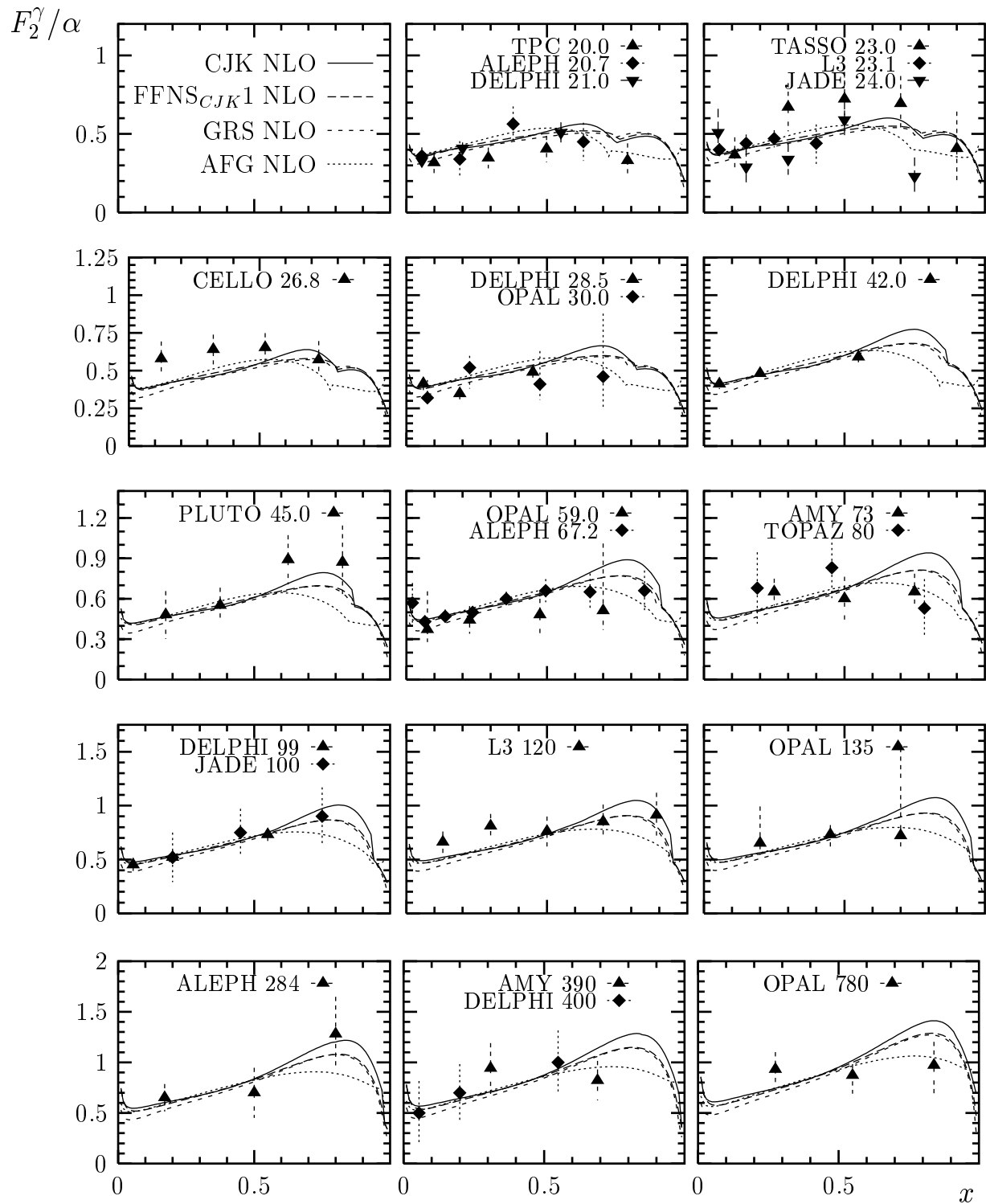


Figure 9: The same as in Fig. 7 for a linear scale in  $x$ .

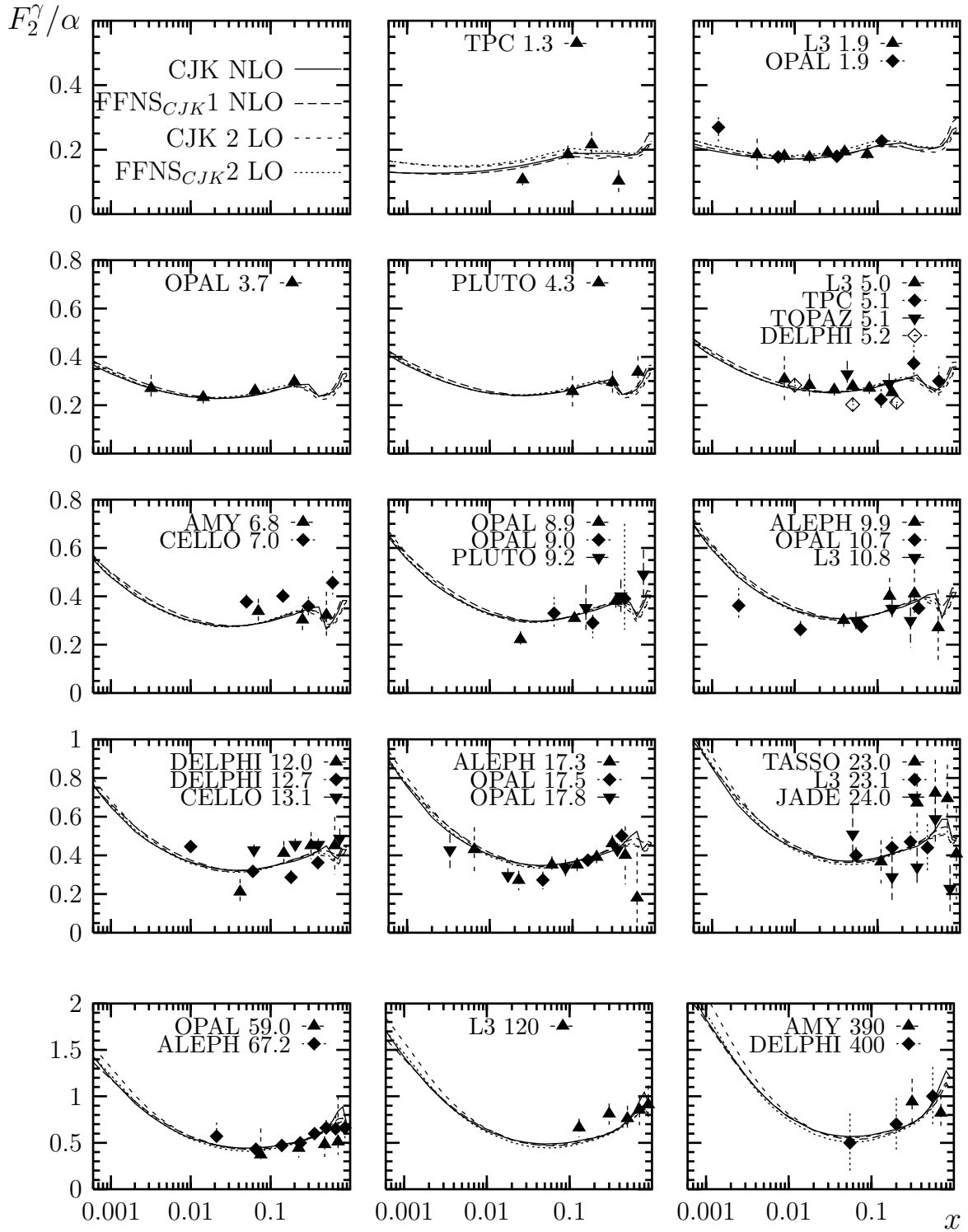


Figure 10: Predictions for the  $F_2^\gamma(x, Q^2)/\alpha$  for the CJK NLO and  $FFNS_{CJK}$  NLO models compared with corresponding LO fits from [2] and with the experimental data [23]–[36], for small and medium  $Q^2$  as a function of  $x$  (logarithmic scale). If a few values of  $Q^2$  are displayed in the panel, the average of the smallest and biggest  $Q^2$  was taken in the computation.

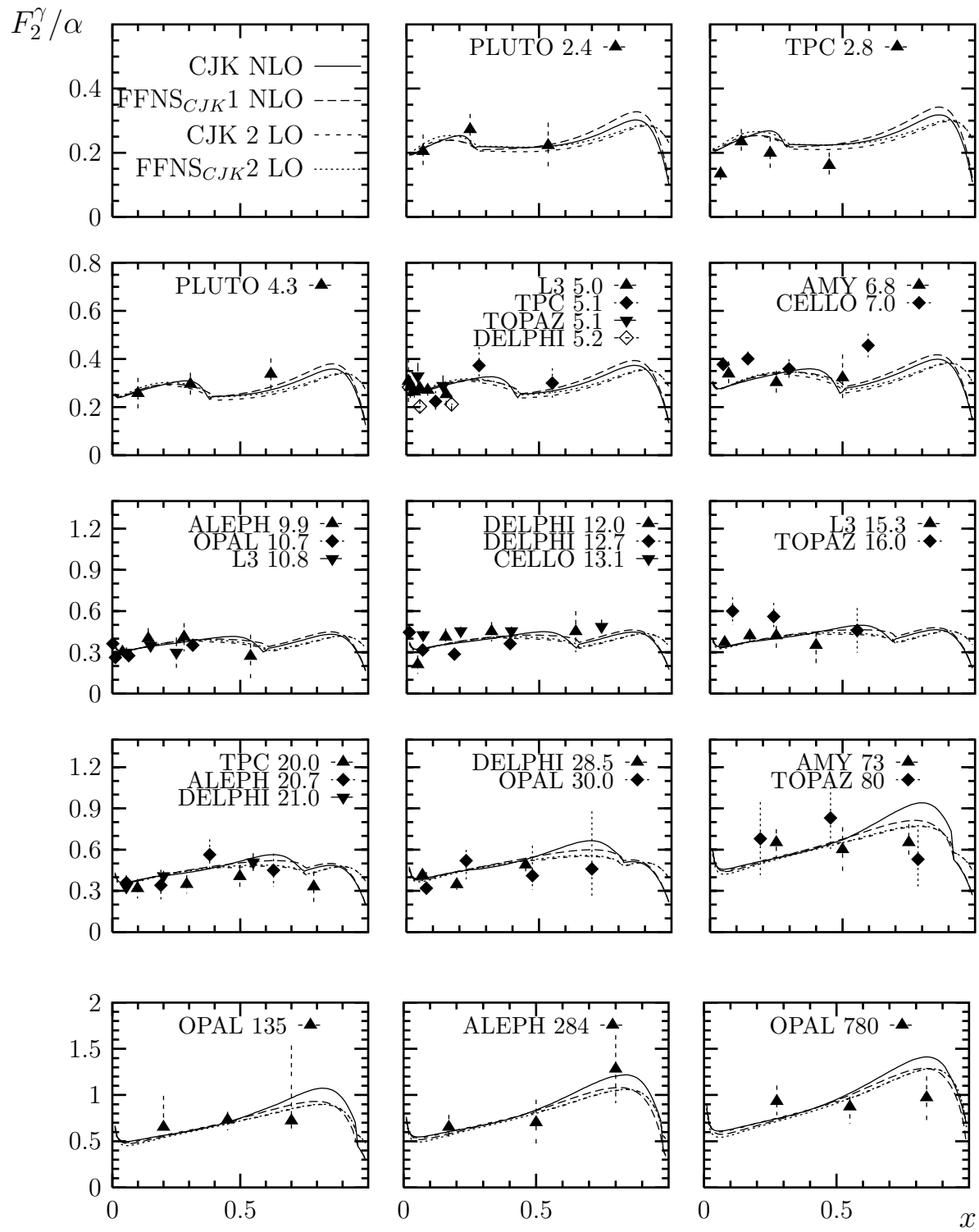


Figure 11: The same as in Fig. 10 for a linear scale in  $x$ .

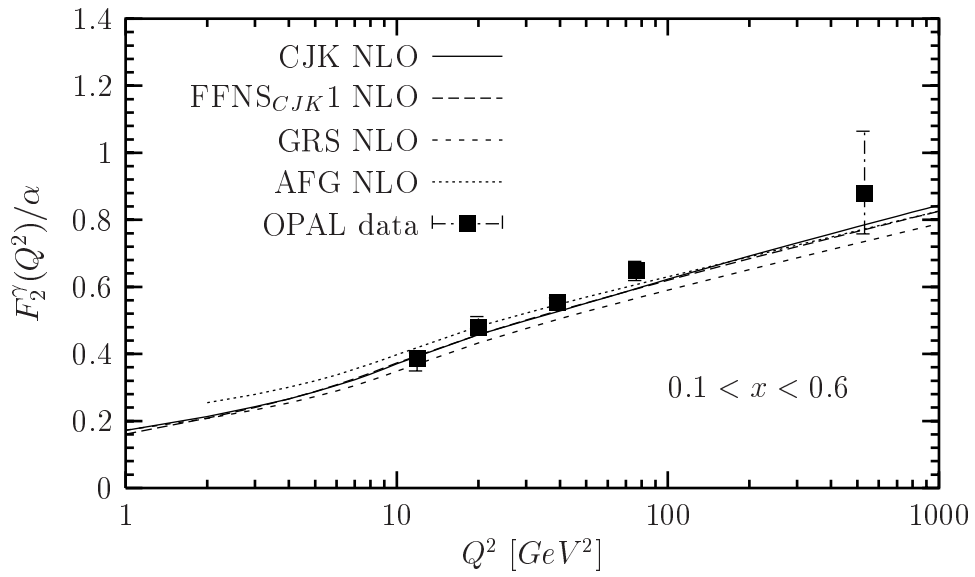


Figure 12: Comparison of the OPAL data [36] for the  $Q^2$ -dependence of the averaged over  $0.1 < x < 0.6$   $F_2^\gamma/\alpha$  with the predictions of the CJK NLO and FFNS<sub>CJK</sub> NLO models.

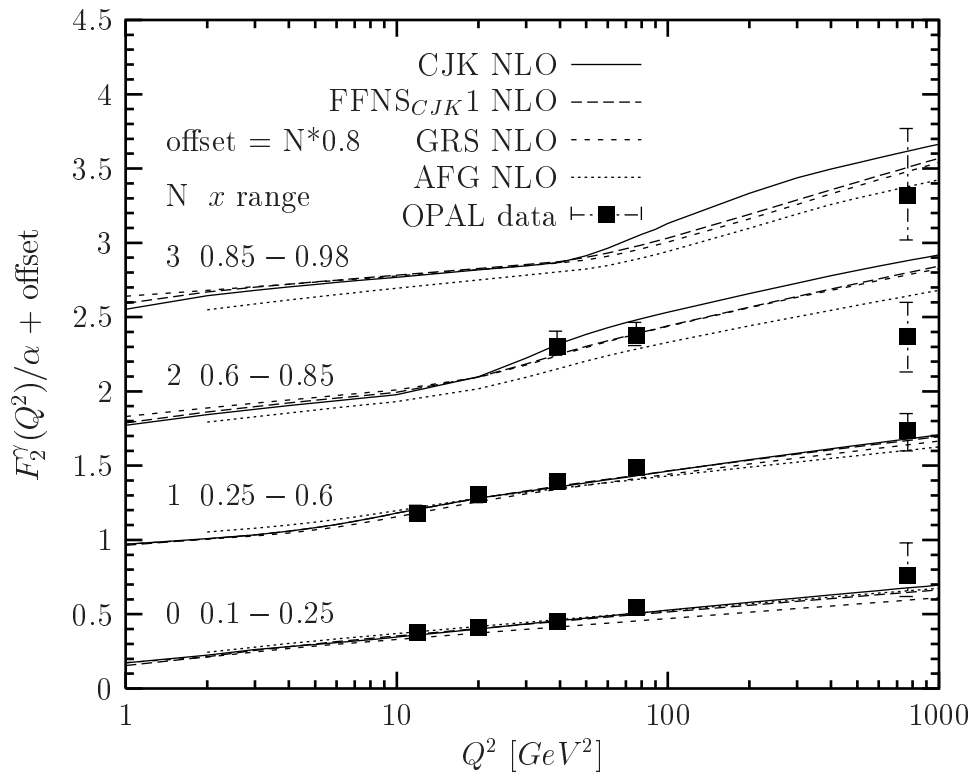


Figure 13: As in Fig. 12 for  $F_2^\gamma(x, Q^2)/\alpha$ , averaged over four different  $x$  ranges.

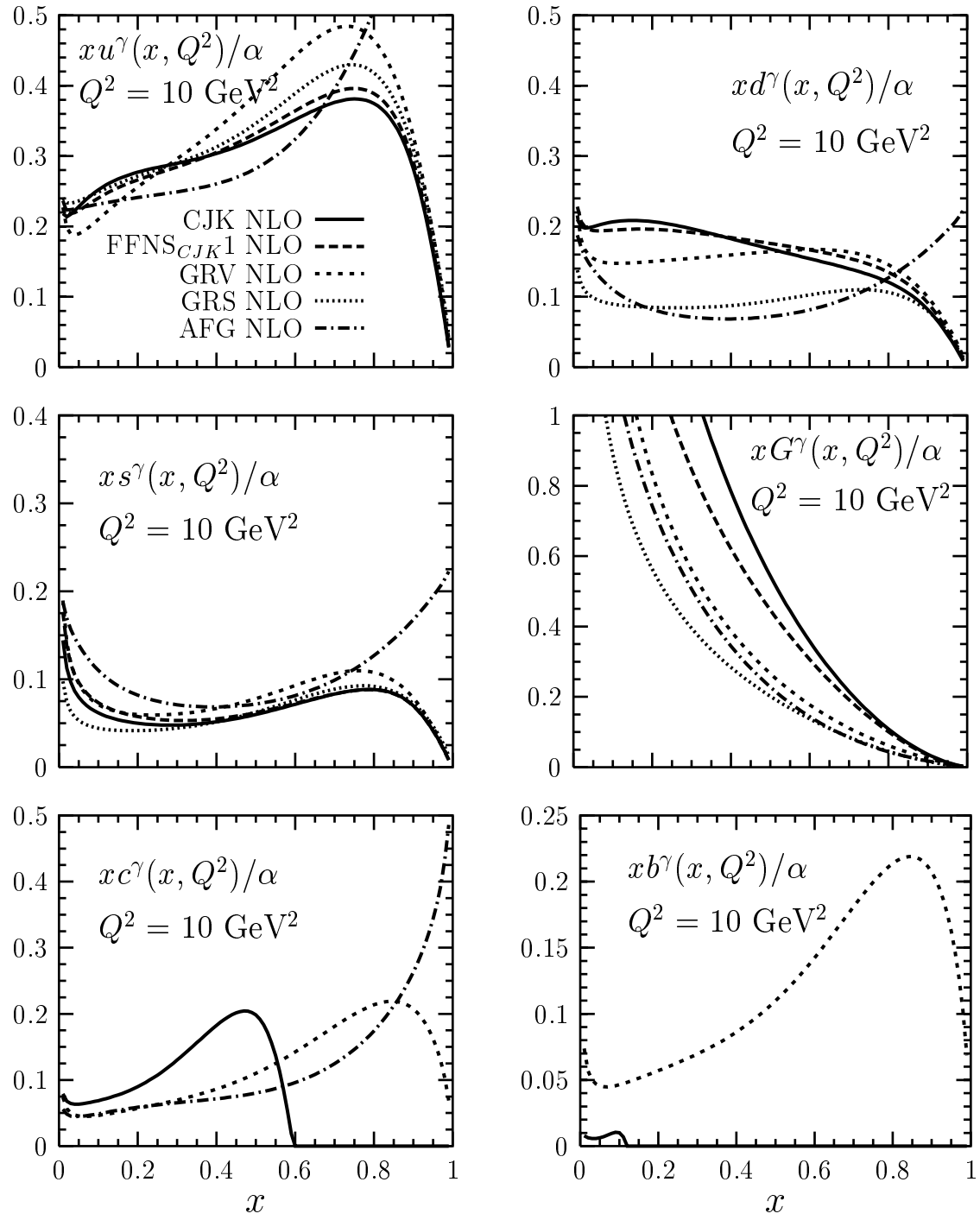


Figure 14: Comparison of the NLO parton densities predicted by CJK NLO and FFNS<sub>CJK1</sub> NLO models and by GRV NLO [7], GRS NLO [8] and AFG NLO [43] parametrizations at  $Q^2 = 10 \text{ GeV}^2$ , as a function of  $x$ .

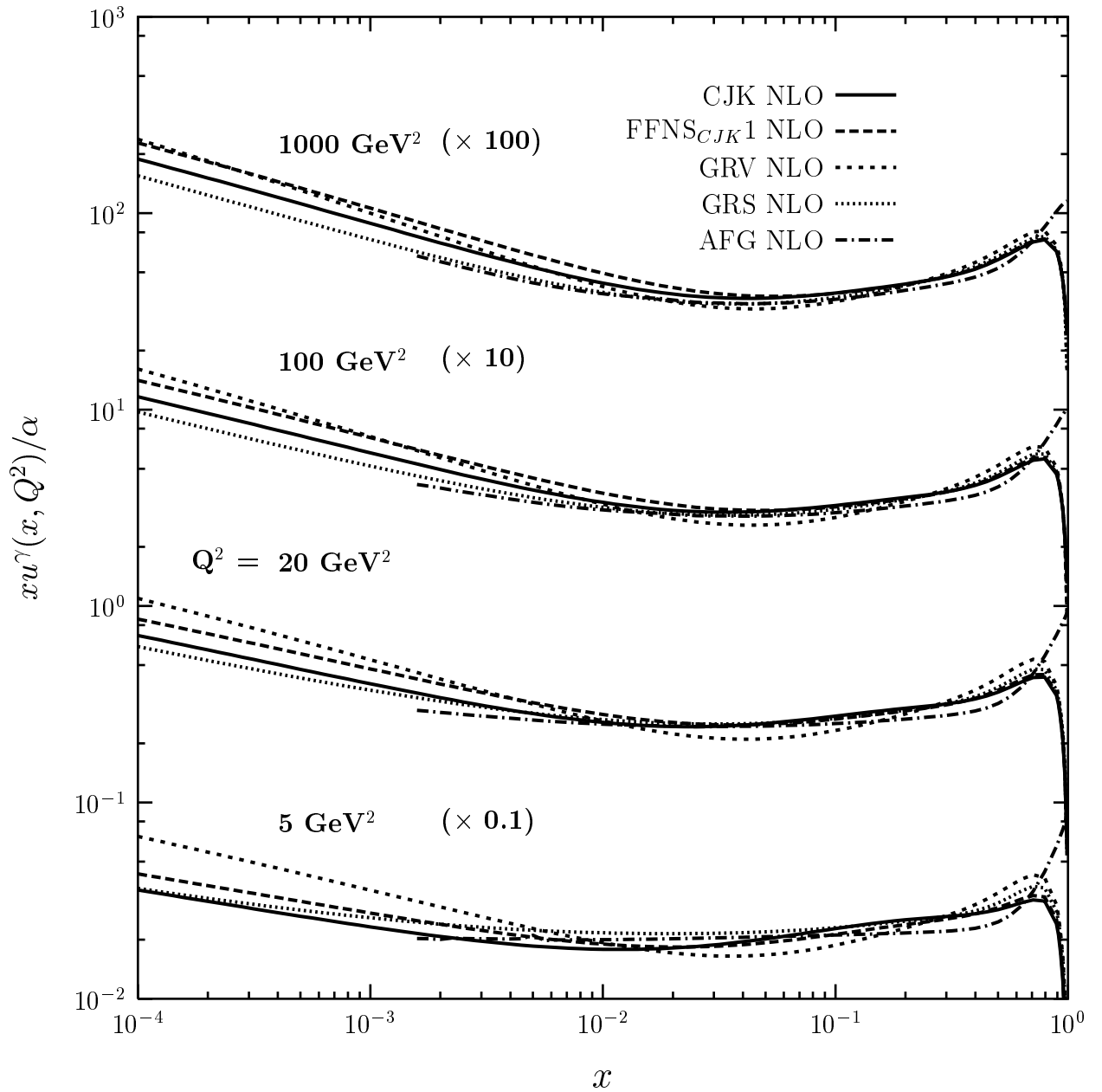


Figure 15: Comparison of the up-quark density at four values of  $Q^2$  in the CJK and  $\text{FFNS}_{\text{CJK1}}$  NLO models with the GRV NLO [7], GRS NLO [8] and AFG NLO [43] densities.

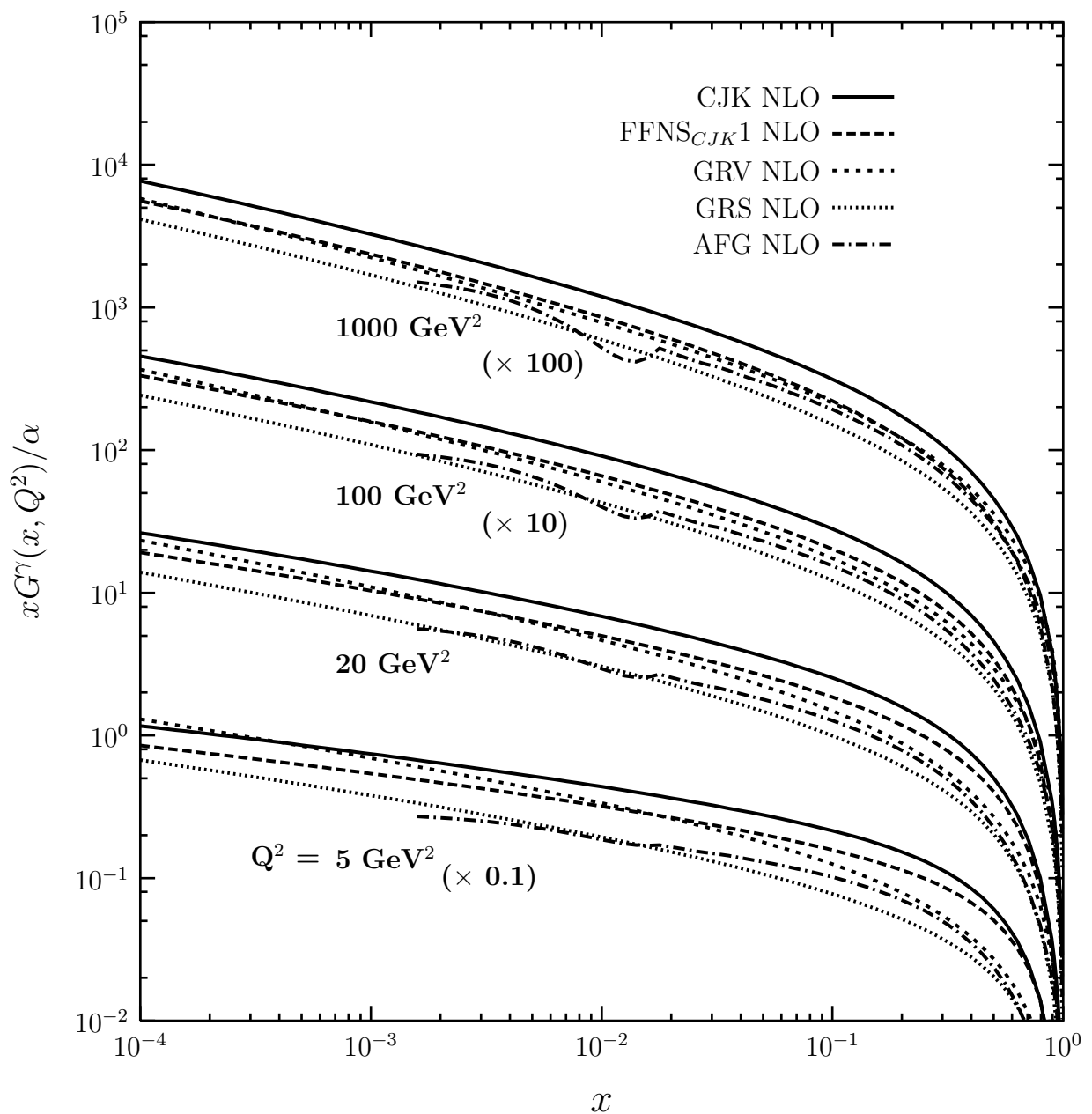


Figure 16: The same as in Fig. 15 for the gluon density.

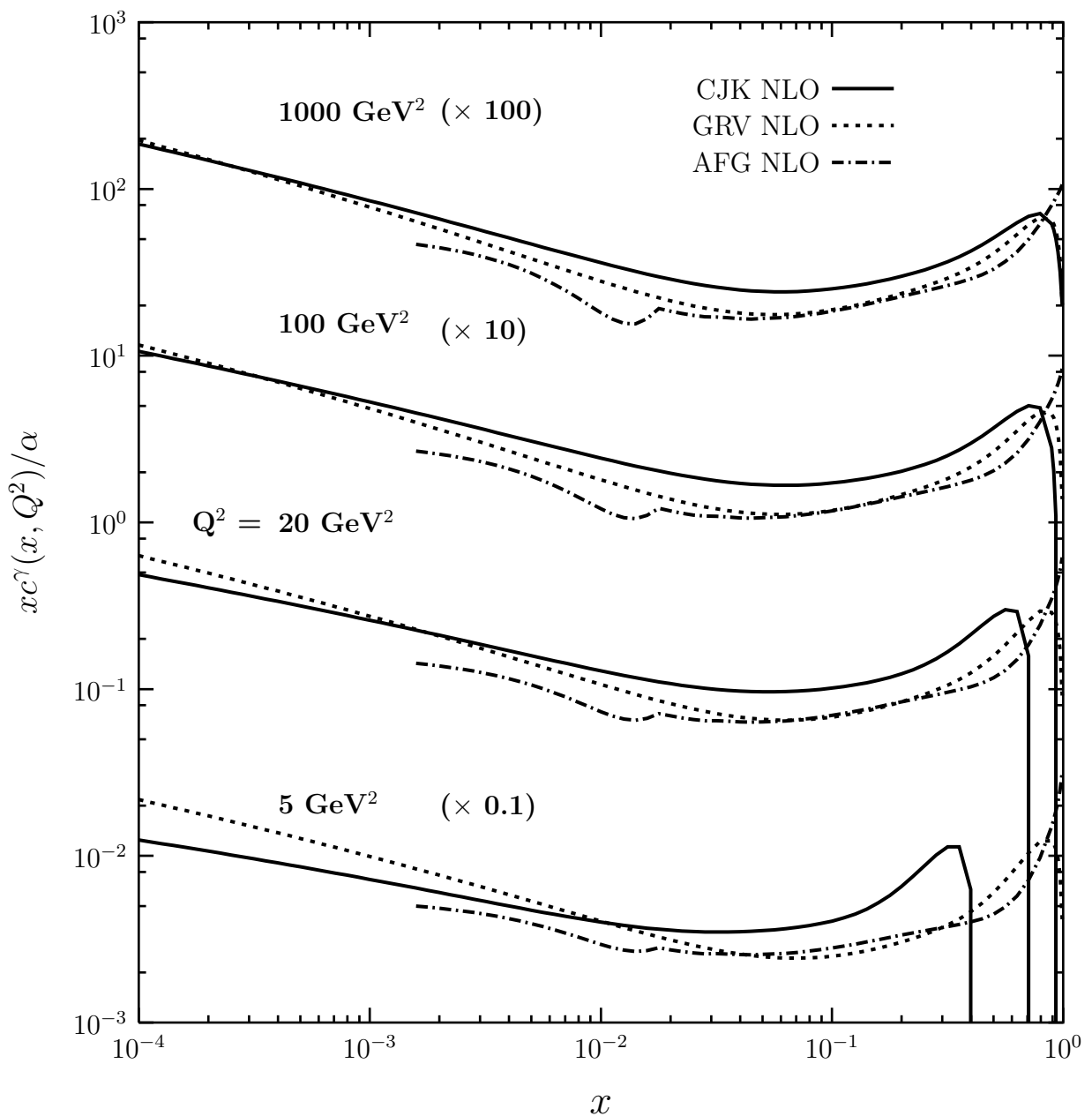


Figure 17: The same as in Fig. 15 for the charm-quark density.

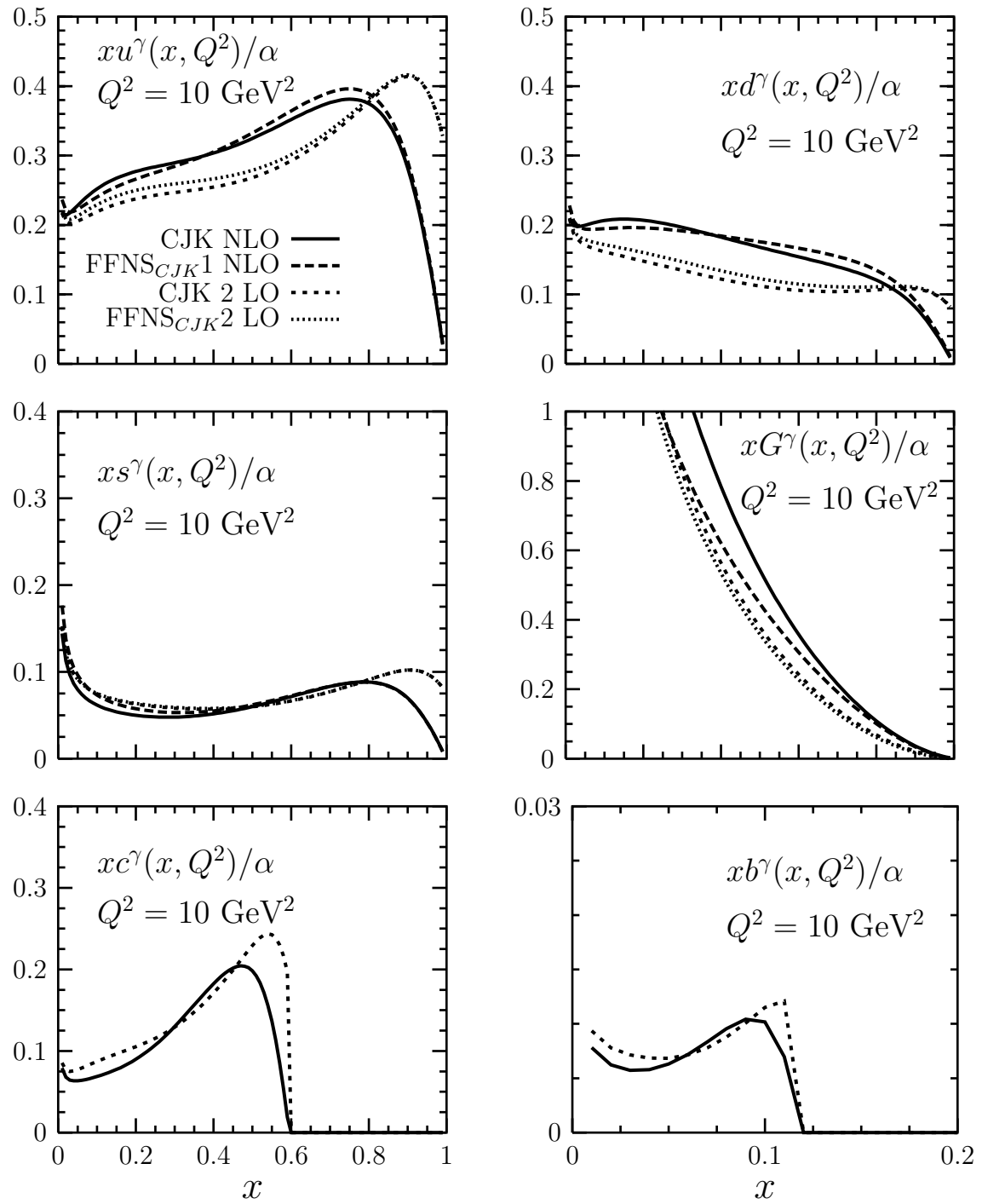


Figure 18: Comparison of the parton densities predicted by the CJK NLO and FFNS<sub>CJK1</sub> NLO models and by corresponding LO models, CJK LO and FFNS<sub>CJK2</sub> LO (i.e. including the resolved-photon  $\gamma^*G \rightarrow h\bar{h}$  contribution) from [2] at  $Q^2 = 10 \text{ GeV}^2$ , as a function of  $x$ .

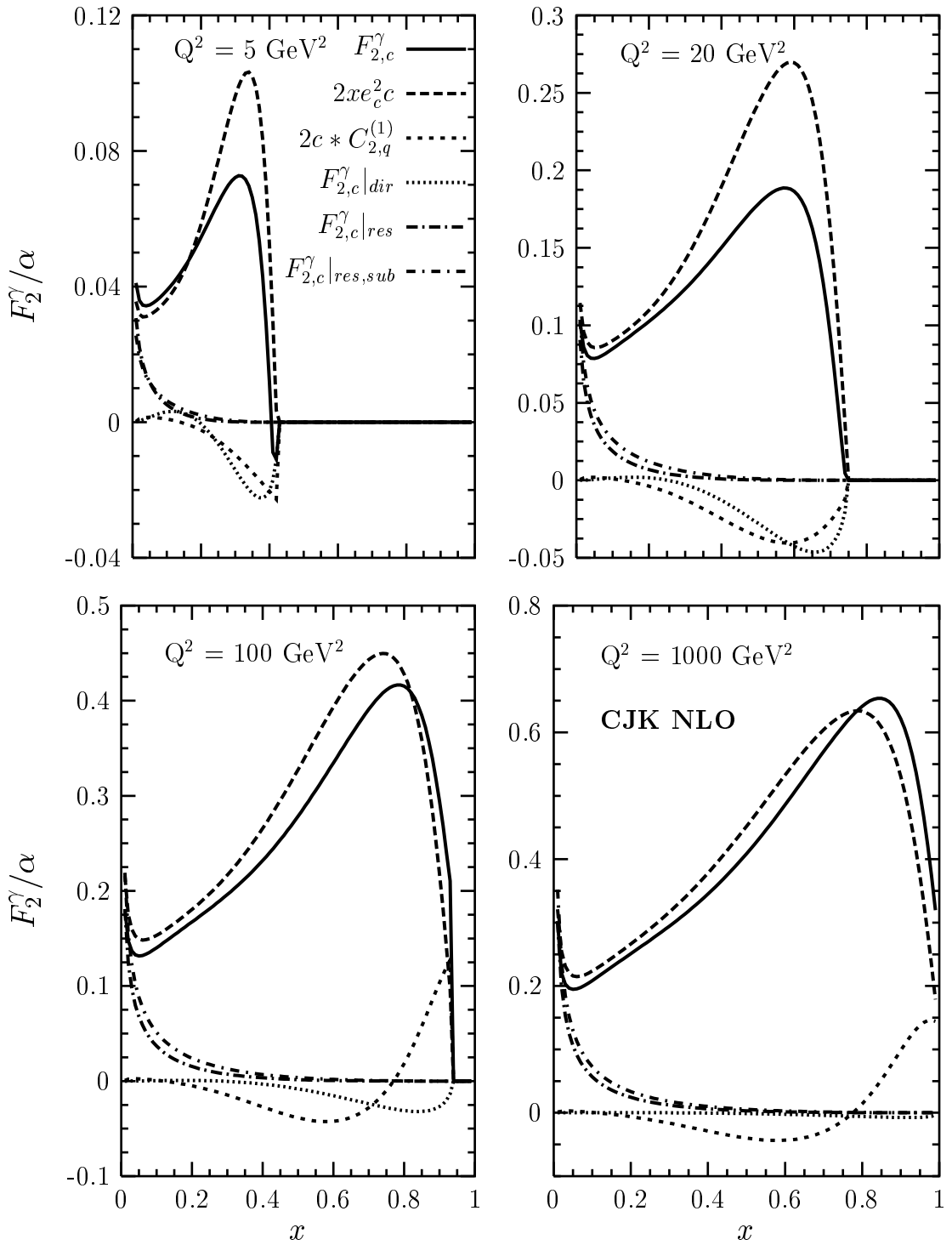


Figure 19: Comparison of various contributions to the photon structure function  $F_{2,c}^{\gamma}(x, Q^2)/\alpha$  in the CJK NLO model for  $Q^2 = 5, 20, 100$  and  $1000 \text{ GeV}^2$ .

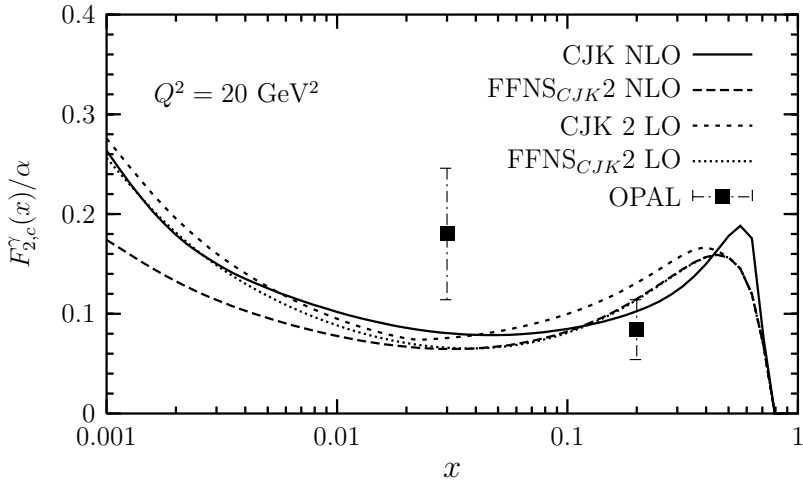


Figure 20: Comparison of the structure function  $F_{2,c}^\gamma(x, Q^2)/\alpha$  calculated in the CJK and FFNS<sub>CJK</sub> models for NLO & LO with the OPAL measurement [44].

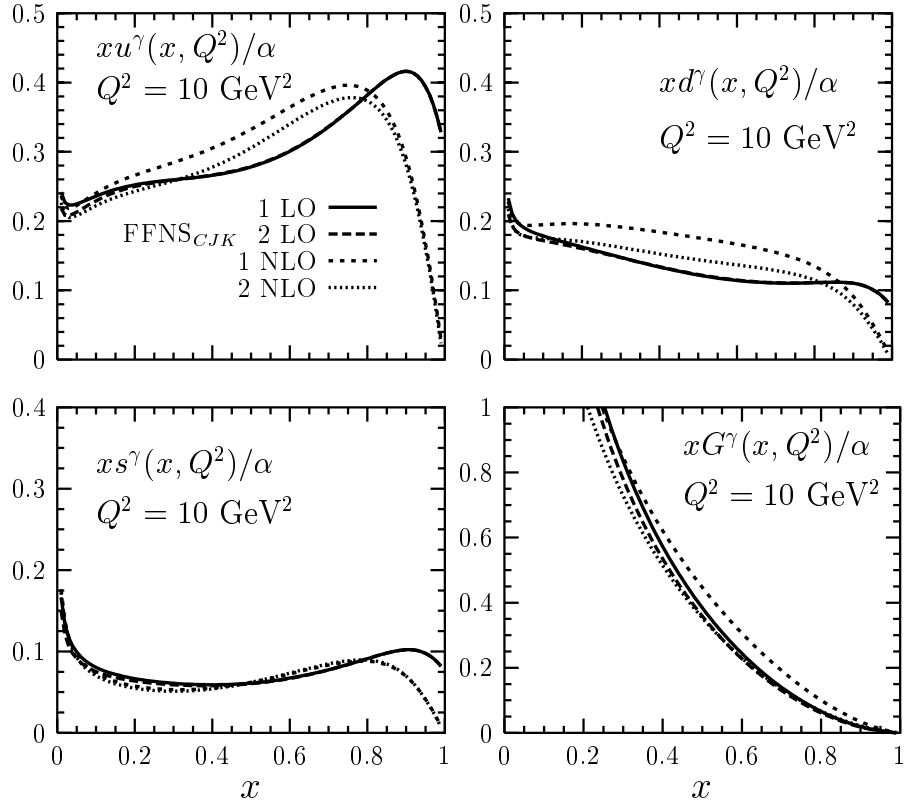


Figure 21: Comparison of the parton densities predicted by the FFNS<sub>CJK</sub> 1 & 2 NLO models and by the corresponding FFNS<sub>CJK</sub> 1 & 2 LO models presented in [2] at  $Q^2 = 10 \text{ GeV}^2$ , as a function of  $x$ .

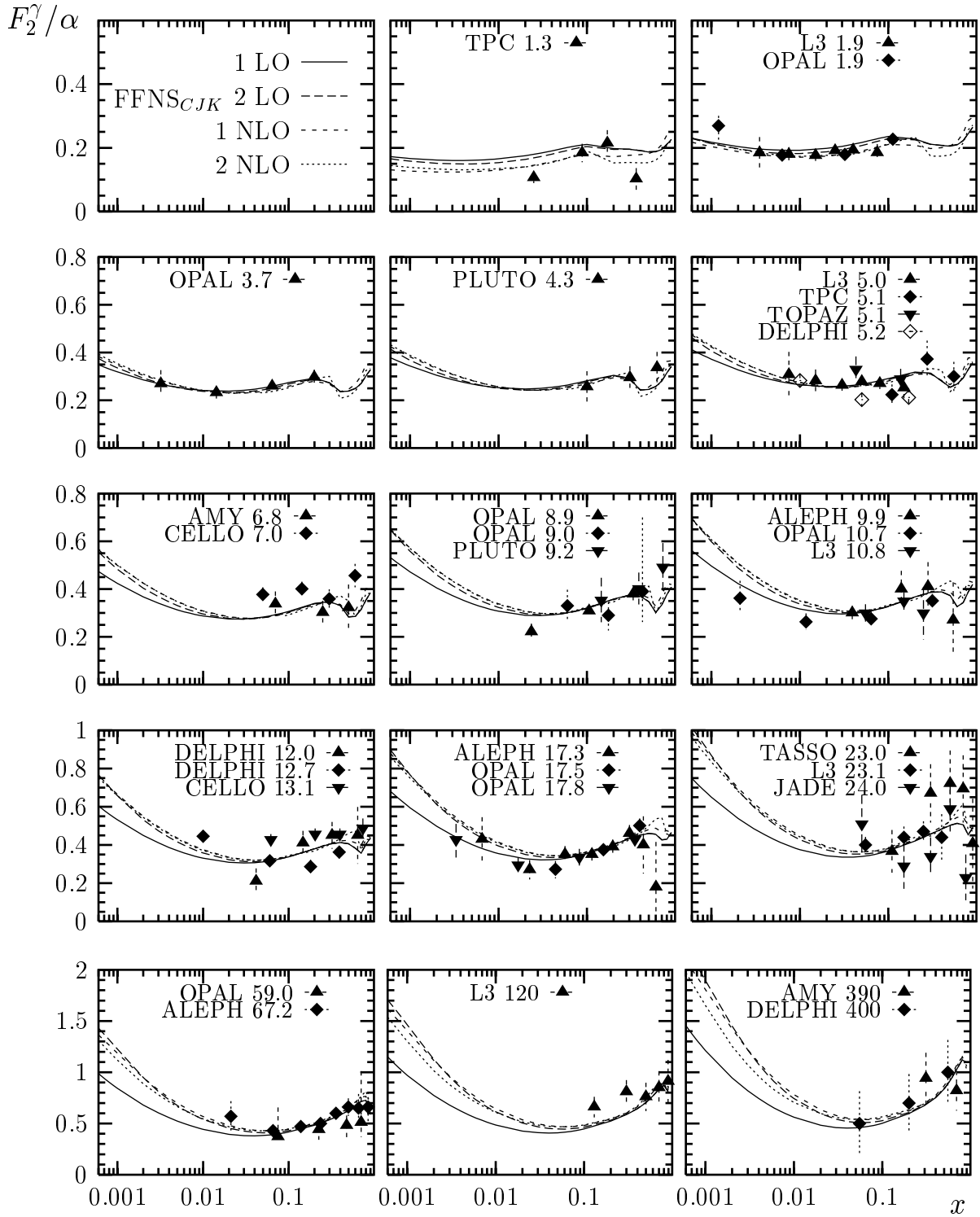


Figure 22: Predictions for the  $F_2^\gamma(x, Q^2)/\alpha$  for the  $FFNS_{CJK}$  models, as in Fig. 21, compared with the corresponding LO fits from [2] and with the experimental data [23]–[36], for small and medium  $Q^2$  as a function of  $x$  (logarithmic scale). If a few values of  $Q^2$  are displayed in the panel, the average of the smallest and biggest  $Q^2$  was taken in the computation.

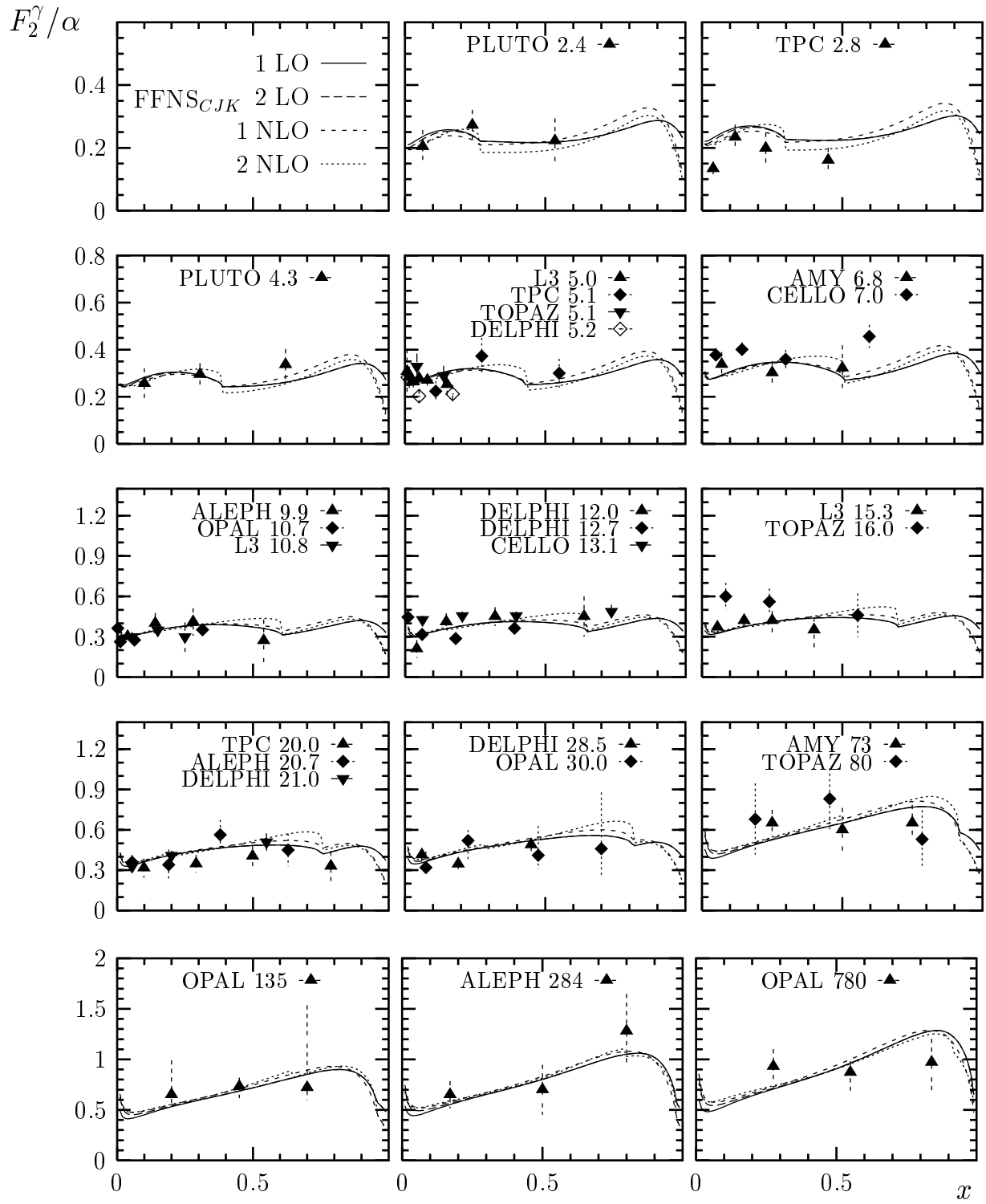


Figure 23: The same as in Fig. 22 for a linear scale in  $x$ .

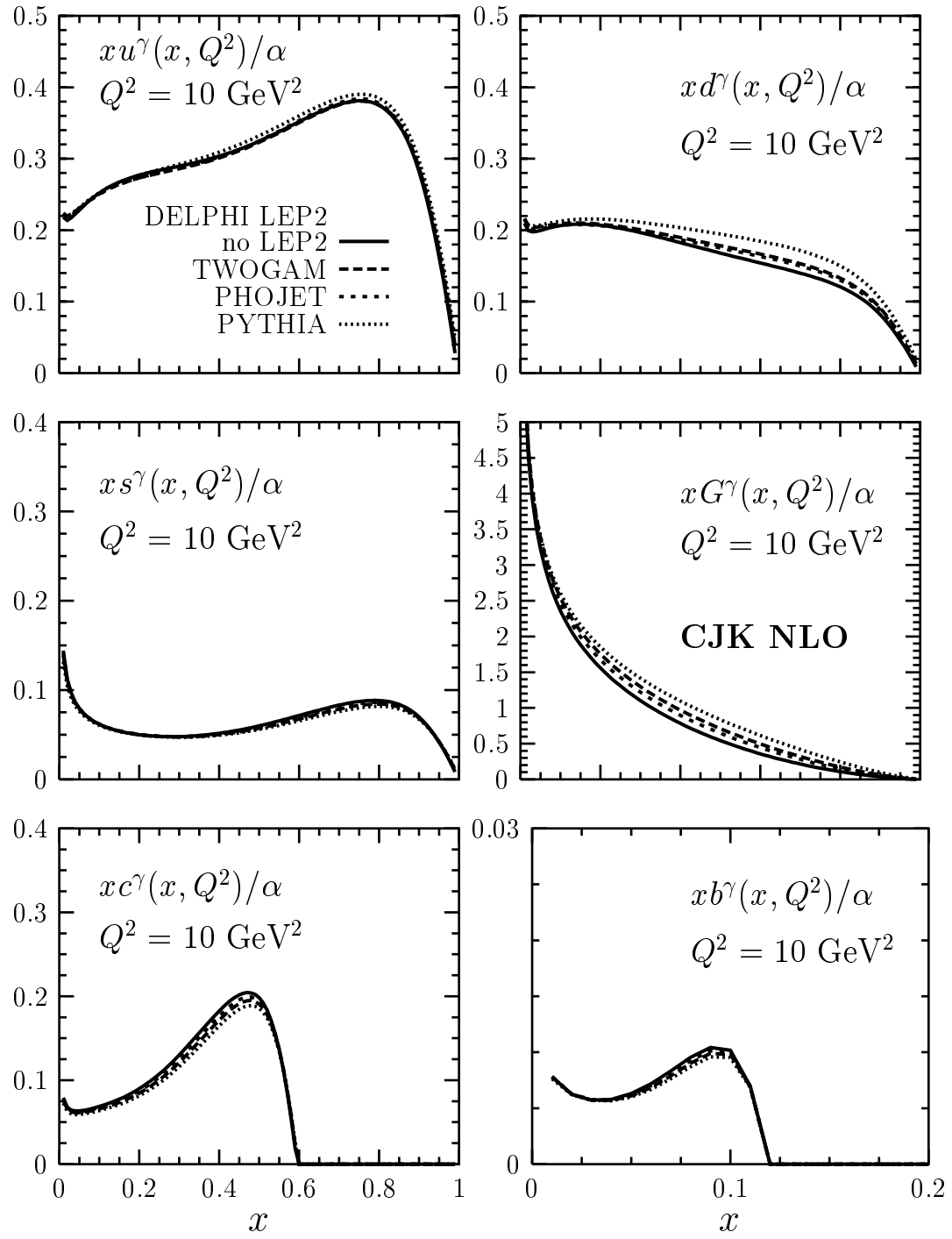


Figure 24: Comparison of the parton densities predicted by the test fits obtained with the CJK NLO model using various sets of the DELPHI LEP2 data [31] at  $Q^2 = 10 \text{ GeV}^2$ , as a function of  $x$ .

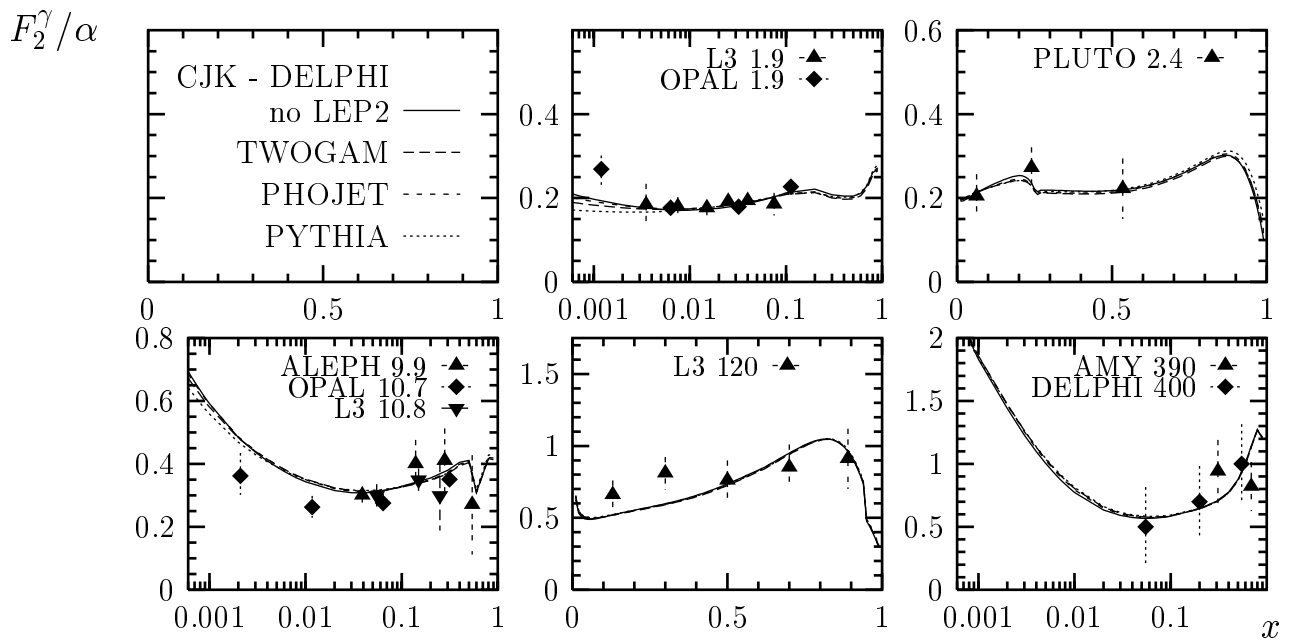


Figure 25: Predictions for the  $F_2^\gamma(x, Q^2)/\alpha$  for the CJK NLO model obtained in the test fits using various sets of the DELPHI LEP2 data [31].